Master Thesis

The effect of disorder on the axial anomaly in a lattice model in 1 + 1 dimensions

Agnes Wattrang

Condensed matter theory, Department of Physics,
School of Engineering Sciences
Royal Institute of Technology, SE-106 91 Stockholm, Sweden

Stockholm, Sweden 2023

Typeset in LaTeX

TRITA–SCI-GRU 2023:018
© Agnes Wattrang, March 2023
Printed in Sweden by Universitetsservice US AB, Stockholm March 2023

Abstract

This work investigates the effect of a disorder potential, that represents impurities/dislocations in the lattice, on the time-dependent signature of the axial anomaly in a one-band tight-binding model in one spatial dimension. The tight-binding model is solved numerically and the simulation results are compared with a semiclassical expression for the time-dependent axial density, $n_5(t)$, due to Nielsen and Ninomiya [1]. An estimate of the scattering time, which enters into the semiclassical expression, is computed using the Fermi golden rule (FG) approximation. The inclusion of disorder in the lattice model, in the form of a random disorder potential with Gaussian correlations, alters the time evolution of the axial density, from being oscillating in the clean case, to a curve that saturates at a non-zero value in the presence of sufficiently strong disorder. The semiclassical result is in accordance with the numerical solution in most of the parameter regimes considered. The FG approximation appears to be more accurate in the moderate to strong disorder regime than in the weak regime (in contrast with the validity condition of the FG approximation). A possible extension of the model in 1 + 1 dimensions to a model in 3 + 1 dimensions is briefly discussed.

Key words: Axial anomaly, tight-binding model, semiclassical physics, correlated disorder.

Sammanfattning

I detta arbete undersöks verkan av en störningspotential, som representerar orenheter i gittret, på tidsutvecklingen hos den axiala/kirala anomalin i en tätbindningsmodell i en rumsdimension. Modellen löses numeriskt och simuleringsresultaten jämförs med Nielsen och Ninomiyas [1] semiklassiska uttryck för den tidsberoende axiala densiteten, $n_5(t)$. Relaxationstiden för spridningseffekter, vilken ingår i det semiklassiska uttrycket, beräknas med hjälp av Fermis gyllene regel. När modellen utsätts för en störning, i form av en korrelerad stokastisk potential, ändras tidsutvecklingen för den axiala densiteten, från att vara oscillerande i det rena fallet, till en kurva som saturerar vid ett nollskilt värde i närvaro av en tillräckligt stark störning. Det semiklassiska resulatet överensstämmer med den numeriska lösningen i majoriteten av de paramterregimer som beaktas. Fermis gyllene regel stämmer bättre överens med simuleringsresultaten för ett system utsatt för en måttlig till kraftig störning än för ett svagt stört system (vilket strider mot giltighetsvillkoret för Fermis gyllene regel). En möjlig utvidging av modellen i 1 + 1 dimensioner till en modell i 3 + 1 dimensioner diskuteras i korthet.

Nyckelord: Axial/kiral anomali, tätbindningsmodell, semiklassisk fysik, korrelerad oordning.

Acknowledgments

I would like to thank my two supervisors, Professor Jens H. Bardarson and Julia D. Hannukainen, for introducing me to this subject. I would like to thank them for their guidance and help during the process of writing the thesis.

Contents

Abstract . . . iii
Sammanfattning . . . iii

Acknowledgments **v**

Contents **vii**

1 Introduction **1**

2 Theoretical background **5**
2.1 The tight-binding approximation . . . 5
2.2 The semiclassical model of electron dynamics . . . 7
2.2.1 Bloch oscillations . . . 8
2.3 The 1D tight-binding model with an applied electric field . . . 10
2.4 An approximate analytical expression for the axial density . . . 12
2.5 The Nielsen and Ninomiya result . . . 14

3 The clean system **16**
3.1 The Schrödinger equation in momentum space . . . 16
3.2 A formula for the axial density in terms of expansion coefficients . 17
3.3 Numerical results . . . 18

4 The disordered system **24**
4.1 The disorder potential . . . 24
4.2 Scattering rate . . . 26
4.3 Energy scales . . . 27
4.4 Numerical results . . . 28

5 Conclusion **33**

Appendices **35**

A A formula for the axial density in terms of expansion coefficients **36**

B Time evolution of a product state with a non-interacting Hamiltonian 38

C Numerical method 41

D The disorder potential 43

E Reduced units 45

Bibliography 45

Chapter 1

Introduction

A quantum anomaly refers to the phenomenon where a symmetry of a classical theory does not adhere to the quantized theory [2–5]. Such a broken symmetry entails the non-conservation of a corresponding physical quantity. In the case of the axial anomaly, the axial symmetry is broken in the quantized theory, which leads to the non-conservation of the axial vector current, j_5^μ, as well as the non-conservation of the right-handed and left-handed chiral currents, j_R^μ and j_L^μ, respectively [2–6]. Please note that throughout this introductory chapter Planck's reduced constant $\hbar$ and the speed of light c are set equal to unity.

The notion of chirality refers to right-chiral and left-chiral objects, e.g. particles or fields representing particles [5, 7, 8]. For massless particles, the notion of chirality coincides with that of helicity. The latter is defined as the projection of spin onto momentum, with corresponding operator (called the helicity operator) given by $\hat{h} \equiv \frac{\vec{p}\cdot\vec{\sigma}}{|\vec{p}|}$, where $\vec{p}$ is the particle's three-momentum, and $\vec{\sigma} = (\sigma^1, \sigma^2, \sigma^3)$ is the vector of Pauli matrices [5, 7, 8]. A massless particle with spin and momentum aligned is called a right-handed particle whereas a massless particle with spin and momentum in opposite directions is called a left-handed particle.

A massless non-interacting Dirac field satisfies the Weyl equation [3, 5, 7]:

$$i\gamma^\mu \partial_\mu \psi(x) = 0, \tag{1.1}$$

where $\psi(x)$ is the Dirac wave function, which in $(3 + 1)$-dimensional spacetime is a 4-component complex vector function, and the spacetime point $x = (x^0, x^1, x^2, x^3) = (t, x, y, z)$ (summation over a repeated index ($\mu = 0, 1, 2, 3$) is implied in Eq. (1.1)). The γ^μ are a set of 4×4 Dirac matrices satisfying the Clifford algebra

$$\{\gamma^\mu, \gamma^\nu\} = 2g^{\mu\nu}\mathbf{1}_{4\times 4} \tag{1.2}$$

$$g^{\mu\nu} = \mathrm{diag}(1, -1, -1, -1). \tag{1.3}$$

In the classical (unquantized) theory, Eq. (1.1) is invariant not only under a vector transformation

$$\psi(x) \to e^{i\theta}\psi(x), \tag{1.4}$$

but also under an axial transformation

$$\psi(x) \rightarrow e^{i\gamma_5\theta}\psi(x), \tag{1.5}$$

where θ is an arbitrary constant, and γ_5 is a 4×4 matrix given by $\gamma_5 \equiv i\gamma^0\gamma^1\gamma^2\gamma^3$ [3, 5, 7]. The symmetries in Eqs. (1.4) and (1.5) correspond to two conserved quantities, the vector current, j^μ, and the axial vector current, j_5^μ, respectively. These currents are defined as [3, 5, 6]:

$$\begin{aligned} j^\mu(x) &\equiv j_R^\mu(x) + j_L^\mu(x) \equiv \bar{\psi}(x)\gamma^\mu\psi(x) && (1.6)\\ j_5^\mu(x) &\equiv j_R^\mu(x) - j_L^\mu(x) \equiv \bar{\psi}(x)\gamma^\mu\gamma_5\psi(x), && (1.7)\end{aligned}$$

where j_R^μ and j_L^μ are the right-handed and left-handed currents, corresponding to right-handed and left-handed Weyl fermions and $\bar{\psi} \equiv \psi^\dagger\gamma^0$ is the conjugate Dirac field. The currents in Eqs. (1.6) and (1.7) are separately conserved when ψ is treated as a classical field. This means that the currents satisfy continuity equations [2–5]:

$$\partial_\mu j^\mu = 0, \quad \partial_\mu j_5^\mu = 0, \quad \partial_\mu j_R^\mu = 0, \quad \partial_\mu j_L^\mu = 0. \tag{1.8}$$

The axial and chiral anomalies emerge upon quantization of the Dirac field [3, 5]. Consider the massless Dirac field in Eq. (1.1) coupled to a vector gauge field A_μ. The equation of motion for ψ then reads [3, 8]:

$$\gamma^\mu(i\partial_\mu - eA_\mu(x))\psi(x) = 0, \tag{1.9}$$

where A_μ is the electromagnetic 4-vector potential and $-e$ is the electronic charge. Equation (1.9) possesses both vector symmetry and axial symmetry in the unquantized theory, and the corresponding currents, j^μ and j_5^μ, are thus conserved. In the quantized theory, however, where the field ψ is treated as a quantum field operator, vector symmetry and axial symmetry cannot be simultaneously preserved, and as a consequence, the vector current, j^μ, and the axial vector current, j_5^μ, are not separately conserved [2, 3, 5]. The reason for this symmetry breaking, and the corresponding non-conservation of one of the two currents, stems from the quantization condition of the Dirac field [3, 5]:

$$\{\psi_m^\dagger(x), \psi_n(y)\} = \psi_m^\dagger(x)\psi_n(y) + \psi_n(y)\psi_m^\dagger(x) = \delta_{mn}\delta(x-y), \tag{1.10}$$

where m and n label the components of $\psi^\dagger$ and ψ. The anticommutator in Eq. (1.10) is singular when the fields ψ and $\psi^\dagger$ are evaluated at the same spacetime point. The vector current and the axial vector current contain bilinears of the Dirac field at the same spacetime point and are therefore not well-defined in the quantized theory. In order to well-define j^μ and j_5^μ a so-called regularization procedure is needed [2, 3, 5]. Such a method introduces a regulator (a "cutoff") which makes it possible to cancel out the unwanted singularities from the quantum theory. A consequence of the regularization procedure is however that the regularized quantum field theory does not simultaneously respect vector symmetry and axial symmetry when the massless

Dirac field is coupled to a gauge field A_μ [2, 3, 6]. In that case, a choice has to be made regarding which one of the two symmetries that ought to be preserved. The choice is dependent on what type of physical system is under investigation. In those problems where preservation of vector symmetry is chosen over axial symmetry the regularized quantum field theory acquires axial and chiral anomalies. The axial vector current is then no longer conserved and the anomalous dynamical equation for j_5^μ reads [2, 3, 5, 6]:

$$\partial^\mu j_\mu^5 = \frac{e^2}{16\pi^2} \varepsilon^{\mu\nu\alpha\beta} F_{\mu\nu} F_{\alpha\beta} \sim \vec{E} \cdot \vec{B}, \tag{1.11}$$

where $F_{\mu\nu}$ is the electromagnetic field strength tensor, $F_{\mu\nu} \equiv \partial_\mu A_\nu - \partial_\nu A_\mu$, and $\varepsilon^{\mu\nu\alpha\beta}$ is the Levi-Civita symbol. The corresponding equations for the right-handed and left-handed currents are given by

$$\partial^\mu j_\mu^R = \frac{1}{2} \frac{e^2}{16\pi^2} \varepsilon^{\mu\nu\alpha\beta} F_{\mu\nu} F_{\alpha\beta} \tag{1.12}$$

$$\partial^\mu j_\mu^L = -\frac{1}{2} \frac{e^2}{16\pi^2} \varepsilon^{\mu\nu\alpha\beta} F_{\mu\nu} F_{\alpha\beta}. \tag{1.13}$$

The number of right-handed and left-handed massless Dirac particles are thus not separately conserved in the regularized quantum field theory. Quantum corrections explicitly break axial symmetry, thus preventing the separate conservation of the right-handed and left-handed chiral particles. The external electromagnetic fields work as a pump that transmutes right-handed particles into left-handed ones, or vice versa [9]. The result is a current of chiral particles whose dynamics is described by Eqs. (1.11)-(1.13).

The earliest theoretical predictions regarding the axial anomaly were made in 1949 in the study of the decay of a neutral pion to two photons ($\pi^0 \to \gamma\gamma$) in a pion-nucleon (π-N) model [2]. It was not until 1969, however, that the anomaly became more well-understood, following the publications of Bell and Jackiw on the one hand, and Adler on the other [6, 10]. The former performed a study of the decay $\pi^0 \to \gamma\gamma$ in the σ-model and found that the process violates the presumed partial conservation of the axial-vector current (PCAC) [10]. The resolution to this"puzzle", as the authors termed it, lay in a modification of the regularization of the quantum theory. Adler, on his side, examined the axial-vector vertex in spinor electrodynamics [6]. He showed that within the framework of perturbation theory the axial-vector vertex displays anomalous properties which do not tally with the corresponding properties obtained from a direct manipulation of the field equations. One of the anomalous properties consists in an additional term in the expression for the divergence of the axial-vector current, the term on the right-hand side of Eq. (1.11), which has come to be called the Adler-Bell-Jackiw (ABJ) anomaly after its founders.

Nielsen and Ninomiya reformulated the theory by Adler, Bell and Jackiw to a condensend matter setting in their letter *The Adler-Bell-Jackiw anomaly and Weyl* *fermions in a crystal* published in 1983 [1]. In this work Nielsen and Ninomiya show how the anomaly emerges in a condensend matter system as the production of Weyl-like fermions (fermions in the massless limit), and use the result to show that there is no net production of such particles in chirally invariant lattice theories. The authors further point to an analogy between the Weyl fermion theory and gapless semiconductors in which two energy bands touch at isolated points (points of degeneracy) in energy-momentum space to form a Dirac cone. When such materials are subjected to parallel electric and magnetic fields a transfer of electrons in energy-momentum space occurs, from the vicinity of one degeneracy point to another one—an effect analogous to the ABJ anomaly on a lattice.

The aim of this master thesis project is to examine the effect of disorder on the time-dependent signature of the axial anomaly in a lattice model in $1 + 1$ dimensions. To this end, the model studied is a one-band tight-binding model of non-interacting (spinless) electrons on a one-dimensional lattice under the influence of an applied electrostatic field. The model presented is a strongly simplified one, not aimed to describe any real material with Weyl-like properties. Yet the model can be used to study features of the anomaly that may, with some modifications, be applicable to three-dimensional materials. The inclusion of disorder in the lattice model aims to mimic the impurities and lattice defects that are present in real materials. These defects are realized as an on-site random disorder potential in the tight-binding Hamiltonian describing the system. In order to study the time evolution of the system, the Schrödinger equation, expressed in the plane-wave basis states, is solved numerically.

Chapter 2

Theoretical background

2.1 The tight-binding approximation

The tight-binding approximation (TBA) is probably the most commonly used approximation when it comes to the quantum mechanical description of electrons in solids. Please note that throughout this text, the word 'electrons' always refers to the conduction electrons, unless otherwise stated. The main assumption of the TBA is that the electrons of a solid are tightly bound to the ion cores, and that the former have a small, but non-vanishing, probability amplitude of tunneling or "hopping" to neighbouring atoms [11, 12]. The essence of the approximation lies in that the electrons are tightly bound to the ion cores that form the lattice, this in contrast to the other extreme where the electrons are weakly bound to the ion cores—the nearly-free electron model. This means that it is very unlikely to find an electron which resides in between lattice sites (i.e. the ion cores). Consequently, there is no need to consider the wave function that describes the electrons in other positions than at the lattice sites (since away from the lattice sites the wave function can be assumed to be zero). That is, instead of trying to solve the Schrödinger equation

$$H\Psi(\mathbf{r}) = E\Psi(\mathbf{r}), \tag{2.1}$$

where the single-particle Hamiltonian is given by

$$H = \frac{\mathbf{p}^2}{2m} + V(\mathbf{r}) = -\frac{\hbar^2\boldsymbol{\nabla}^2}{2m} + V(\mathbf{r}), \tag{2.2}$$

one reduces the complexity of the problem from trying to compute the entire (spatial) probabilty density, $P(r) = |\Psi(r)|^2$, to only computing the probability of finding the particle in one of the lattice sites. Historically, one of the most commonly found applications of the TBA is the calculation of the electronic band structure of solids. The model is best suited to describe the d bands of the transition metals and the electronic band structure of insulators [13, 14].

Consider a crystal of N atoms with one orbital per atom. The TBA assumes that the influence of one atom on the others in the system is small so that the atomic orbitals remain approximately undistorted [11]. This assumption, together with the assumption that an electron in the solid is strongly localized to a single ion between two events of tunneling, is taken into account when constructing an approximate wave function for the electron. The one-electron wave function is approximated as a sum of atomic orbitals

$$\psi_{\mathbf{k}}(\mathbf{r}) = \frac{1}{\sqrt{N}} \sum_j e^{i\mathbf{k}\cdot\mathbf{r}_j} \varphi(\mathbf{r} - \mathbf{r}_j), \tag{2.3}$$

where $\varphi(\mathbf{r} - \mathbf{r}_j)$ is the atomic orbital centered at the jth atom and the sum extends over all atoms in the system. This form of the wave function fulfils the Bloch theorem, which states that the solutions to the Schrödinger equation in a periodic potential are given by plane waves times a periodic function [11, 13]:

$$\psi_{\mathbf{k}}(\mathbf{r}) = e^{i\mathbf{k}\cdot\mathbf{r}} u_{\mathbf{k}}(\mathbf{r}), \tag{2.4}$$

where the function $u_{\mathbf{k}}(\mathbf{r})$ has the periodicity of the crystal lattice and the wavevector $\mathbf{k}$ is restricted to the first Brillouin zone. The corresponding state

$$|\psi_{\mathbf{k}}\rangle = \frac{1}{\sqrt{N}} \sum_j e^{i\mathbf{k}\cdot\mathbf{r}_j} |j\rangle \tag{2.5}$$

is an eigenstate of the crystal with energy eigenvalue given by

$$\epsilon_{\mathbf{k}} = \langle \psi_{\mathbf{k}} | H | \psi_{\mathbf{k}} \rangle . \tag{2.6}$$

In order to evaluate the matrix element in Eq. (2.6), the crystal potential $V(\mathbf{r})$ in the Hamiltonian in Eq. (2.2) is written as a sum of the individual atomic potentials

$$V(\mathbf{r}) = \sum_j v(\mathbf{r} - \mathbf{r}_j) = v(\mathbf{r} - \mathbf{r}_j) + \Delta v_j, \tag{2.7}$$

where $v(\mathbf{r} - \mathbf{r}_j)$ is the atomic potential due to the atom at position $\mathbf{r}_j$ in the lattice and $\Delta v_j \equiv \sum_{j' \neq j} v(\mathbf{r} - \mathbf{r}_{j'})$ is that due to the rest of the atoms. The matrix element in Eq. (2.6) is given by

$$\langle \psi_{\mathbf{k}} | H | \psi_{\mathbf{k}} \rangle = \varepsilon_0 + \frac{1}{N} \sum_{j,j'} e^{i\mathbf{k}\cdot(\mathbf{r}_j - \mathbf{r}_{j'})} \langle j' | \Delta v_j | j \rangle , \tag{2.8}$$

where ε_0 is the atomic energy eigenvalue. The treatment is here restricted to hoppings between nearest neighbour atoms and the following notation is used

$$\langle j' | \Delta v_j | j \rangle = \begin{cases} \Delta\varepsilon & \text{if} \quad j = j' \\ -t_1 & \text{if } j' \text{ is a nearest neighbour of } j \\ 0 & \text{otherwise.} \end{cases} \tag{2.9}$$

The quantity $\Delta\varepsilon$ is assumed to be small since the contribution from Δv_j is assumed to be small in the vicinity of the jth atom. In the following it is assumed that

$\Delta\varepsilon \simeq 0$. The parameter t_1 is called the overlap or transfer integral and determines the probability that an electron will tunnel or "hop" to a neighbouring atom. The total energy of an electron in the crystal is given by

$$\epsilon_{\mathbf{k}} = \varepsilon_0 - t_1 \sum_{\boldsymbol{\delta}} e^{-i\mathbf{k}\cdot\boldsymbol{\delta}}, \tag{2.10}$$

where $\boldsymbol{\delta} = \mathbf{r}_{j'} - \mathbf{r}_j$ is a vector that connects two neighbouring lattice sites. In one spatial dimension, i.e. in a tight-binding chain, the nearest neighbour atoms are located at $\boldsymbol{\delta} = \pm a\hat{x}$ (a is the lattice constant). The dispersion relation of the electron is in this case given by

$$\epsilon_{\mathbf{k}} = \varepsilon_0 - 2t_1 \cos(ka). \tag{2.11}$$

A plot of the dispersion relation is shown in Fig. 2.1.

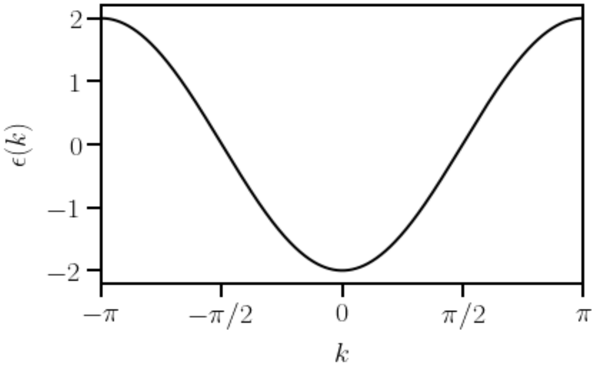

Figure 2.1: Energy spectrum of an electron in a tight-binding chain. The atomic energy is set to zero ($\varepsilon_0 = 0$). The tunneling amplitude and the lattice constant are both set to unity ($t_1 = a = 1$).

2.2 The semiclassical model of electron dynamics

The semiclassical model treats the dynamics of Bloch electrons, i.e. the dynamics of electrons in a periodic potential. As stated in the previous section, the solutions to the periodic Schrödinger equation are given by

$$\psi_{n\mathbf{k}}(\mathbf{r}) = e^{i\mathbf{k}\cdot\mathbf{r}} u_{n\mathbf{k}}(\mathbf{r}), \tag{2.12}$$

where the functions $u_{n\mathbf{k}}(\mathbf{r})$ have the periodicity of the crystal lattice. The band index, denoted by n in Eq. (2.12), is a constant of the motion in the semiclassical description [14]. This means that an electron cannot "jump" between bands in this picture. In the forthcoming discussion the band index is omitted and the focus will be only on one band.

In the absence of impurities and lattice distortions, such as line dislocations, the electrons in a crystal travel collisionlessly throughout the material—a fact due to quantum interference, which is a quantum mechanical phenomenon that allows the wavefunction to interfere with itself [11]. This enables a quantum particle to simultaneously occupy more than one spatial position, as well as it renders it possible for the particle to interfere with its own trajectory.

The electrons of a solid are treated as (semi)classical particles made up of Bloch-state wave packets in the semiclassical description. It can be shown that the group velocity of a Bloch-state wave packet, and hence the average velocity of a Bloch electron in a fixed energy level, is given by [14]:

$$\mathbf{v}_g(\mathbf{k}) = \hbar^{-1}\boldsymbol{\nabla}_{\mathbf{k}}\epsilon(\mathbf{k}). \tag{2.13}$$

One of the objectives of the semiclassical model is to describe the effect on the dynamics of the electrons in a periodic potential when the system is subjected to a slowly varying (in space and time) external potential $U(\mathbf{r})$. The Hamiltonian for an electron in the system is then given by

$$H = \epsilon(\mathbf{k}) + U(\mathbf{r}), \tag{2.14}$$

where $\epsilon(\mathbf{k})$ is the one-electron energy in the absence of external fields. The total energy of the electron is conserved, implying that

$$0 = \frac{dH}{dt} = \frac{d\mathbf{k}}{dt}\cdot\boldsymbol{\nabla}_{\mathbf{k}}\epsilon(\mathbf{k}) + \frac{d\mathbf{r}}{dt}\cdot\boldsymbol{\nabla}U(\mathbf{r}). \tag{2.15}$$

Insertion of the expression for the group velocity, i.e. $d\mathbf{r}/dt = \mathbf{v}_g(\mathbf{k})$, in Eq. (2.15) gives

$$\hbar\frac{d\mathbf{k}}{dt} = -\boldsymbol{\nabla}U(\mathbf{r}) = \mathbf{F}. \tag{2.16}$$

Equation (2.16) is the quantum-mechanical analog of Newton's second law of motion. It states that the rate of change of the crystal momentum, $\mathbf{p}_c = \hbar\mathbf{k}$, equals the externally applied force on the electron.

2.2.1 Bloch oscillations

When the force acting on the electron in Eq. (2.16) is given by a constant electric field, and restricting the problem to one spatial dimension, the equation of motion for the electron's crystal momentum reads

$$\hbar\frac{dk}{dt} = -eE, \tag{2.17}$$

where $-e$ and E are the electronic charge and the electric field, respectively. Integrating Eq. (2.17) gives

$$k(t) = k(0) - \frac{eEt}{\hbar}, \tag{2.18}$$

which shows that the crystal momentum increases linearly in time. This is however not the whole picture, since the wavevector really is periodic in reciprocal space, which means that $k(t)$ is a bounded function (see Fig. 2.2 (a)). This fact has the implication for the electronic motion that when the electron reaches the Brillouin zone boundary, i.e. $k = \pm\pi/a$ in $d = 1$, it will immediately reappear at the opposite zone boundary. The explanation to this is that the electron is Bragg reflected back to the opposite zone boundary [11]. Figure 2.2 (b) shows the k-space velocity of a Bloch electron exposed to a constant electric field. The dispersion relation of the electron is given by Eq. (2.11). The average velocity of the electron, $v(k) \sim \sin{(ka)}$, is approximately linear near the band minimum. Half-way to the zone boundary, the electron is decelerated by the applied electric field, so that the velocity drops and starts to decrease as $v \sim -k$. At the zone boundary the velocity vanishes as a result of the Bragg reflection. After being Bragg reflected to the opposite zone boundary the electron continues to descend the band at that side of the Brillouin zone. The electron will in this manner describe an oscillatory motion, which in case of more than one electron, gives rise to an oscillating current. The phenomenon as such is referred to as *Bloch oscillations.* The motion of the electron(s) is oscillatory in real space as well. The real-space position of the electron in the semiclassical model is given by [13]:

$$\langle x(t)\rangle = \int v_g(k(t))\,dt = -\frac{2t_1}{eE}\Big(\cos\Big(\frac{eEat}{\hbar}\Big) - 1\Big), \tag{2.19}$$

where the initial condition is set to $\langle x(0)\rangle = 0$. This shows that the amplitude of the Bloch oscillations scales as the inverse of the applied electric field and that the frequency of the oscillations is given by $\omega_B = eEa/\hbar$. The latter is called the Bloch frequency. Note that the period of a Bloch oscillation, i.e. the time it takes for an electron to traverse the Brillouin zone once, which of course is consistent with the period in Eq. (2.19), is obtained from Eq. (2.18) as

$$\tau_B = \frac{2\pi/a}{eE/\hbar} = \frac{2\pi\hbar}{eEa} = \frac{2\pi}{\omega_B}. \tag{2.20}$$

It has proven very difficult to observe Bloch oscillations in experiment due to scattering of the electrons from impurities and thermal lattice vibrations. The requirement that has to be met in order to see Bloch oscillations in experiment is that the scattering time τ (the time between two consecutive scattering events) is much larger than the period of a Bloch oscillation, i.e. $\tau \gg \tau_B$, so that the electron(s) is able to perform many oscillations before being scattered. This is hard to achieve in most materials; lately Bloch oscillations have however been observed in semiconductor superlattices [15, 16].

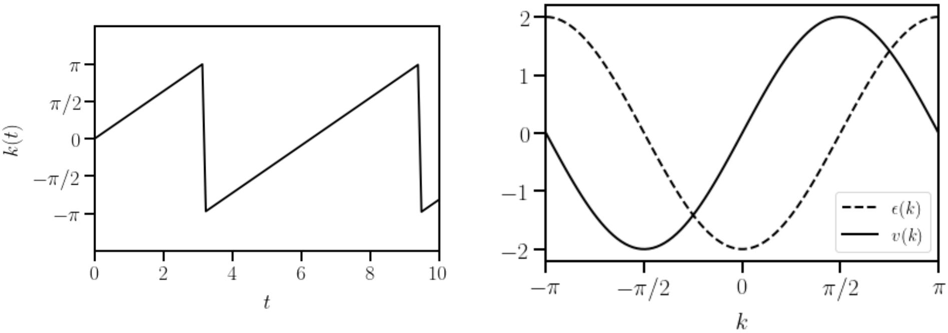

(a)

(b)

Figure 2.2: Semiclassical dynamics. (a) Time dependence of the k-vector in the presence of an external electric field. (b) k-space velocity of a Bloch electron in a constant electric field (solid line), plotted toghether with the dispersion relation of an electron in a tight-binding chain (dashed line). In both figures the electric field strength $E = 1$, in reduced units. The tight-binding parameters are given by $\varepsilon_0 = 0$ and $t_1 = a = 1$. The elementary charge and Planck's reduced constant are both set to unity, $e = \hbar = 1$.

2.3 The 1D tight-binding model with an applied electric field

The intention in this section is to write down the simplest lattice model that captures the essential physics of the axial anomaly in a condensed matter system, as outlined by Nielsen and Ninomiya in their article *The Adler-Bell-Jackiw anomaly and Weyl fermions in a crystal* [1]. For this purpose, a system of N number of non-interacting spinless [1] electrons confined to move in one spatial dimension is considered. More specifically, the model system considered is a one-dimensional monatomic crystal with N atoms. The quantization length is $L = Na$. It is assumed that the only atomic orbital of relevance is the 1s orbital, which can hold at most two electrons, one with spin up and the other with spin down. In case of spinless electrons this modifies so that the 1s orbital can hold at most one electron since no distinction is made between spin up and spin down in this case. It is furthermore assumed that the electrons can tunnel only between neighbouring lattice sites. Periodic boundary conditions are applied to the system so that the site at position $N + 1$ in the lattice is identified with the first site. The motion of a single electron in the crystal can then be described by the following tight-binding

---

[1] The Pauli exclusion principle is still assumed to hold, i.e. no more than one electron can occupy a distinct quantum state.

Hamiltonian

$$\hat{H} = -t_1 \sum_{i=1}^{N} (\hat{c}_i^\dagger \hat{c}_{i+1} + \text{h.c.}), \tag{2.21}$$

where $\hat{c}_i^\dagger$ and $\hat{c}_i$ are the fermion creation and annihilation operators in second quantization, t_1 is the tunneling amplitude, and h.c. denotes hermitian conjugation. The fermion creation and annihilation operators obey the following anti-commutation relations

$$\{\hat{c}_i, \hat{c}_j^\dagger\} = \delta_{ij}, \qquad \{\hat{c}_i, \hat{c}_j\} = \{\hat{c}_i^\dagger, \hat{c}_j^\dagger\} = 0. \tag{2.22}$$

Physically, the first term on the right-hand side of Eq. (2.21) describes the creation of an electron at site i in the lattice and the annihilation of an electron at site $i+1$, and vice versa for the second term. The tight-binding Hamiltonian is diagonalized by use of the discrete Fourier transforms

$$\hat{c}_j = \frac{1}{\sqrt{N}} \sum_k e^{ikx_j} \hat{c}_k, \qquad \hat{c}_j^\dagger = \frac{1}{\sqrt{N}} \sum_k e^{-ikx_j} \hat{c}_k^\dagger \tag{2.23}$$

$$x_j = aj, \quad j = 1, ..., N, \qquad k_n = \frac{2\pi n}{L}, \quad n = 1, ..., N. \tag{2.24}$$

Substituting for Eq. (2.23) into Eq. (2.21) yields the diagonalized Hamiltonian in momentum space

$$\hat{H} = \sum_k \epsilon(k) \hat{c}_k^\dagger \hat{c}_k, \tag{2.25}$$

where $\epsilon(k) = -2t_1 \cos(ka)$ is the dispersion relation of the electron. Fermions in the massless limit disperse linearly. This is the case e.g. at half-filling in the tight-binding model considered. A plot of the dispersion relation and the linearized dispersion relation at half-filling is shown in Fig. 2.3.

An applied electrostatic field, $\vec{E}(x) = E(x)\hat{x}$, enters the Hamiltonian in Eq. (2.21) in the form of the electrostatic potential, defined as

$$\vec{E}(x) = -\nabla \varphi(x). \tag{2.26}$$

In the case of an uniform electrostatic field

$$\vec{E}(x) = E\hat{x} \quad \Rightarrow \quad \varphi(x) = -Ex. \tag{2.27}$$

The electric potential that enters the Hamiltonian is $V_{el}(x) = -e\varphi(x)$. This gives

$$V_{el}(x = x_i) = eEx_i = eEai \tag{2.28}$$

and the full Hamiltonian reads

$$\hat{H} = \hat{H}_{tb} + \hat{V}_{el} = -t_1 \sum_i (\hat{c}_i^\dagger \hat{c}_{i+1} + \text{h.c.}) + eEa \sum_i i \hat{c}_i^\dagger \hat{c}_i. \tag{2.29}$$

Periodic boundary conditions are applied to this model. The Fourier transform of Eq. (2.29) is given by

$$\hat{H} = -2t_1 \sum_k \cos(ka)\hat{c}_k^\dagger \hat{c}_k + \frac{eEa}{N} \sum_{k,k'} \sum_l l e^{-i(k-k')l} \hat{c}_k^\dagger \hat{c}_{k'}. \tag{2.30}$$

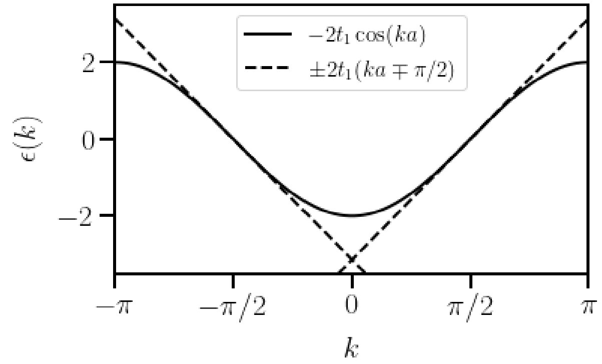

Figure 2.3: Energy spectrum of an electron (solid line) in a tight-binding chain. At half-filling all states below zero are filled, i.e. all states between $k = -\pi/2a$ and $k = \pi/2a$ are filled. The dashed lines show the linearized dispersion relation at half-filling. The tight-binding parameters are set to $\varepsilon_0 = 0$ and $t_1 = a = 1$.

2.4 An approximate analytical expression for the axial density

An approximate analytical expression for the time evolution of the axial density is derived in this section. The derivation is done in the absence of a disorder potential. The result will be used for comparison with the simulation results for the clean system in Sec. 3.3.

The axial density is defined as the difference between the densities of right-handed and left-handed chiral fermions [1, 18]:

$$n_5 = n_R - n_L, \tag{2.31}$$

where n_5 is the axial density, and n_R and n_L are the densities of the right-handed and left-handed chiral fermions. A spinless right-handed chiral fermion has positive average velocity, i.e. $v_g \sim \partial\varepsilon/\partial k > 0$, whereas a spinless left-handed chiral fermion has negative average velocity, $v_g \sim \partial\varepsilon/\partial k < 0$. The total number of right-handed and left-handed chiral electrons are, as a function of time, t, given by

$$N_R(t) = \int_{-\pi/a}^{\pi/a} n(k,t)\,\theta(v_g(k))\,dk = \int_{0}^{\pi/a} n(k,t)\,dk \tag{2.32}$$

$$N_L(t) = \int_{-\pi/a}^{\pi/a} n(k,t)\,\theta(-v_g(k))\,dk = \int_{-\pi/a}^{0} n(k,t)\,dk, \tag{2.33}$$

where θ is the Heaviside step function, $v_g(k)$ is the average electron velocity, and $n(k,t)$ is the electron density. The electron density is given by

$$k_F^{(+)} > k_F^{(-)}: \quad n(k,t) = \begin{cases} L/2\pi & k_F^{(-)}(t) < k < k_F^{(+)}(t) \\ 0 & \text{otherwise} \end{cases} \tag{2.34}$$

$$k_F^{(+)} < k_F^{(-)}: \quad n(k,t) = \begin{cases} L/2\pi & k < k_F^{(+)}(t) \quad \text{or} \quad k > k_F^{(-)}(t) \\ 0 & \text{otherwise,} \end{cases} \tag{2.35}$$

where $k_F^{(\pm)}(t)$ is the Fermi wave vector at time t and $k_F^{(\pm)}(0)$ is the wave vector of the rightmost and leftmost occupied states in the band at the initial time, $t = 0$. The notation $k_F^{(\pm)}$ signifies the Fermi wave vector of the initially right-handed and left-handed electrons at any later time t. The periodicity of the Fermi wave vector is taken into account by expressing it in terms of the floor function:

$$k_F(t) \mod \frac{2\pi}{a} = k_F(t) - \left\lfloor \frac{k_F(t) + \pi/a}{2\pi/a} \right\rfloor \frac{2\pi}{a} \equiv \lfloor k_F(t) \rfloor_{\frac{2\pi}{a}}. \tag{2.36}$$

By this definition $k_F(t)$ is defined within the first Brillouin zone, i.e. $k_F(t) \in [-\pi/a, \pi/a]$. By using the expression for the time-dependent k-vector in Eq. (2.18) $k_F(t)$ can be written as

$$k_F^{(\pm)}(t) = \left\lfloor k_F^{(\pm)}(0) - \frac{eEt}{\hbar} \right\rfloor_{\frac{2\pi}{a}}. \tag{2.37}$$

The time evolution of the axial density is given by

$$n_5(t) = \frac{N_R(t) - N_L(t)}{L}, \tag{2.38}$$

where L in the denominator denotes the system size, and $N_R(t)$ and $N_L(t)$ are given by Eqs. (2.32) and (2.33), respectively. Note that Eq. (2.38) is an implicit expression for the time evolution of the axial density.

The total number of electrons in a band is constant and given by the sum of the number of right-handed and left-handed chiral electrons at any given time t,

$$N_{el} = N_R(t) + N_L(t). \tag{2.39}$$

There is thus not any net production of electrons within the system, only a transfer between electrons of different handedness. Figure 2.4 shows a plot of the time

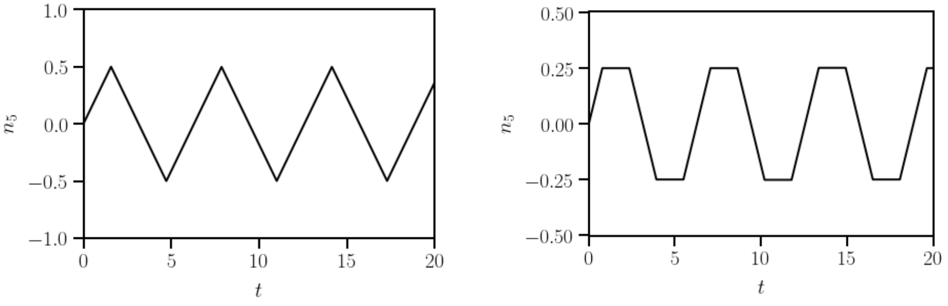

(a) (b)

Figure 2.4: The axial density, n_5, as a function of time, t, at (a) half-filling, and (b) quarter-filling. The plots are based on the expression in Eq. (2.38). The electric field strength $E = 1$ and the lattice constant $a = 1$. The elementary charge and Planck's reduced constant are set to unity, $e = \hbar = 1$.

evolution of the axial density at (a) half-filling and (b) quarter-filling. The plot is based on Eq. (2.38) with the electric field strength set to $E = 1$. The plateaux in the graph in Fig. 2.4 (b) reflect the fact that at the corresponding time intervals there are only right-handed ($n_5 > 0$) or left-handed ($n_5 < 0$) chiral electrons present in the band. The amplitude of the time-dependent chiral density is given by

$$n_{5,amp} = \frac{n_{5,max} - n_{5,min}}{2} = \frac{N_{el}/L - (-N_{el}/L)}{2} = \begin{cases} \frac{\nu}{a} & \nu < 0.5 \\ \frac{1-\nu}{a} & \nu > 0.5, \end{cases} \tag{2.40}$$

where $\nu = N_{el}/N$ is the degree of filling. The amplitude is hence directly proportional to the degree of filling and independent of both the electric field strength and the system size. The electric field strength sets the Bloch frequency, $\omega_B = eEa/\hbar$, which determines the frequency of $n_5(t)$. Here it is also worth pointing out that the amplitude of $n_5(t)$ is the same for a quarter-filled band and for a three-quarter-filled band. This indicates that the behaviour of two systems, one with $\nu = 0.25$, and the other with $\nu = 0.75$, will probably be similar, and that it therefore suffices to investigate the properties of one of them.

2.5 The Nielsen and Ninomiya result

An alternative expression for the time evolution of the axial density can be obtained by appealing to a slightly more physical argument than in the previous section. The following derivation is due to Nielsen and Ninomiya [1]. Consider relativistic Weyl fermions subjected to a constant and uniform electric field in 1 + 1 dimensions. The particles disperse linearly, i.e. $\epsilon(k) \sim \pm k$, and the speed of the particles is given by $dk/dt = \pm eE/\hbar$. The right-handed particles move up the band (are created) at a rate given by

$$\frac{dN_R}{dt} = \frac{dN_R}{dk}\frac{dk}{dt} = \frac{L}{2\pi}\frac{eE}{\hbar} = \frac{eEL}{2\pi\hbar}, \tag{2.41}$$

where $dN_R/dk = L/2\pi$ is the density of states of the number of right-handed particles. Similarly, the left-handed particles move down the band (are annihilated) at a rate given by

$$\frac{dN_L}{dt} = \frac{dN_L}{dk}\frac{dk}{dt} = \frac{L}{2\pi}\Big(-\frac{eE}{\hbar}\Big) = -\frac{eEL}{2\pi\hbar}. \tag{2.42}$$

The rate of change of the axial density is hence given by

$$\frac{dn_5}{dt} = \frac{1}{L}\frac{d(N_R - N_L)}{dt} = \frac{eE}{\pi\hbar}. \tag{2.43}$$

Note that Eq. (2.43) is valid only for short times, since at long times, the axial density $n_5(t)$ grows without a bound according to this expression. To include the effect of disorder in Eq. (2.43) one can simply add a term proportional to the scattering rate to the right-hand side of the equation (relaxation time approximation):

$$\frac{dn_5}{dt} = \frac{eE}{\pi\hbar} - \frac{n_5}{\tau}. \tag{2.44}$$

The solution to Eq. (2.44) is given by

$$n_5(t) = \frac{eE\tau}{\pi\hbar}(1 - e^{-t/\tau}), \tag{2.45}$$

where the initial condition is set to $n_5(0) = 0$. The scattering time, i.e. the time it takes for an electron to scatter from a state with a particular handedness to another state with the opposite handedness, is given by

$$n_{5,\text{steady state}} = \frac{eE\tau}{\pi\hbar} \tag{2.46}$$

where $n_{5,\text{steady state}}$ denotes the steady state value of the axial density for which $dn_5/dt = 0$.

Chapter 3

The clean system

3.1 The Schrödinger equation in momentum space

The time evolution of a quantum mechanical state is given by the Schrödinger equation [21]:

$$i\hbar\frac{\partial \left|\psi(t)\right\rangle}{\partial t} = \hat{H}\left|\psi(t)\right\rangle . \tag{3.1}$$

The momentum-space representation of Eq. (3.1) is obtained by first expanding the state vector in plane wave states according to

$$\left|\psi(t)\right\rangle = \sum_{k} c_k(t)\left|k\right\rangle , \tag{3.2}$$

and then projecting each side of Eq. (3.1) onto momentum space. The projection of each side of Eq. (3.1) onto k-space is given by

$$i\hbar\frac{\partial}{\partial t}\left\langle k|\psi(t)\right\rangle = i\hbar\frac{d}{dt}\sum_{k'} c_{k'}(t)\left\langle k|k'\right\rangle = i\hbar\frac{dc_k(t)}{dt} \tag{3.3}$$

and

$$\langle k|\hat{H}|\psi(t)\rangle = \sum_{k'} \langle k|\hat{H}|k'\rangle\, c_{k'}(t) = \sum_{k'} H_{k,k'}c_{k'}(t). \tag{3.4}$$

Substitution of Eqs. (3.3) and (3.4) into Eq. (3.1) gives the one-electron Schrödinger equation in momentum space

$$i\hbar\frac{dc_k(t)}{dt} = \sum_{k'} H_{k,k'}c_{k'}(t), \qquad c_k(0) = c_k(t_0), \tag{3.5}$$

where $c_k(0) = c_k(t_0)$ is an initial condition. The solution to Eq. (3.5) is given by

$$c_k(t) = \sum_{k'} \hat{U}_{k,k'} c_{k'}(0) = \sum_{k'} (e^{-i\hat{H}t/\hbar})_{k,k'} c_{k'}(0), \tag{3.6}$$

where $\hat{U}_{k,k'}$ is the unitary time evolution operator in momentum space. In order to compute the time evolution of the axial density for a multi-electron system j different equations have to be solved

$$i\hbar \frac{dc_k^j(t)}{dt} = \sum_{k'} H_{k,k'} c_{k'}^j(t), \tag{3.7}$$

where j labels the individual electrons in the system, and the initial condition is set such that the Pauli exclusion principle is satisfied.

3.2 A formula for the axial density in terms of expansion coefficients

In this section an analytical expression for the time-dependent axial density in terms of the expansion coefficients $c_k(t)$ (see Eq. (3.5)) is derived. The expression will be used in the numerical solution of the model.

The one-electron wave function can be written as

$$\psi(x,t) = \frac{1}{\sqrt{L}}\Big(\sum_{k>0} c_k(t)e^{ikx} + \sum_{k<0} c_k(t)e^{ikx}\Big) \equiv \psi_+ + \psi_-, \tag{3.8}$$

where $|\psi_+|^2 \equiv n_R$ and $|\psi_-|^2 \equiv n_L$. The right-handed and left-handed chiral densities are given by

$$\begin{aligned} n_R(x,t) &= \frac{1}{L}\Big|\sum_{k>0} c_k(t)e^{ikx}\Big|^2 = \frac{1}{L}\sum_{k,k'>0} c_k(t)c_{k'}^*(t)e^{i(k-k')x} \\ &= \frac{1}{L}\Big(\sum_{k>0}|c_k(t)|^2 + \sum_{\substack{k\neq k'\\ k,k'>0}} c_k(t)c_{k'}^*(t)e^{i(k-k')x}\Big) \end{aligned} \tag{3.9}$$

and

$$n_L(x,t) = \frac{1}{L}\Big(\sum_{k<0}|c_k(t)|^2 + \sum_{\substack{k\neq k'\\ k,k'<0}} c_k(t)c_{k'}^*(t)e^{i(k-k')x}\Big). \tag{3.10}$$

In order to get rid of the x-dependence in Eqs. (3.9) and (3.10) both sides of the equations are integrated over the system size L and then divided by the same quantity. This yields the following expressions for the electron density and the axial density of a single electron in the system:

$$n(t) = n_R(t) + n_L(t) = \frac{1}{L}\Big(\sum_{k>0} |c_k(t)|^2 + \sum_{k<0} |c_k(t)|^2\Big) \tag{3.11}$$

$$n_5(t) = n_R(t) - n_L(t) = \frac{1}{L}\Big(\sum_{k>0} |c_k(t)|^2 - \sum_{k<0} |c_k(t)|^2\Big). \tag{3.12}$$

When constructing expressions for the axial density and the electron density for the multi-electron system one must take into account the Pauli exclusion principle. The electron density for the multi-electron system is obtained by multiplying the single-electron densities in Eq. (3.12) with an occupation function, which initially is just the Fermi function [11, 22]:

$$f(k) = \frac{1}{e^{\beta(\epsilon(k)-\mu)} + 1}, \tag{3.13}$$

where $\beta = 1/k_B T$, and μ is the chemical potential. The Fermi function gives the probability that the state of energy ϵ is occupied in thermal equilibrium at temperature T. The ground state is defined as the state at absolute zero temperature. In that case $\beta \to \infty$ and the Fermi function becomes a step function:

$$f(k) = \theta(\mu(T=0) - \epsilon(k)) = \theta(\epsilon_F - \epsilon(k)). \tag{3.14}$$

The initial density of the multi-electron system can thus be written

$$n(0) = \frac{1}{L}\sum_{|k|<k_F} |c_k(0)|^2. \tag{3.15}$$

The axial density for the multi-electron system is given by the sum of the axial densities of the individual electrons in the system:

$$n_5(t) = \sum_j n_5^j(t) = \frac{1}{L}\sum_j \Big(\sum_{k>0} |c_k^j(t)|^2 - \sum_{k<0} |c_k^j(t)|^2\Big), \tag{3.16}$$

where the initial state $\{n_5^j(0)\}$ is different for different particles in order to fulfil the Pauli exclusion principle. For a more detailed derivation of this result see Appendix A.

3.3 Numerical results

It is important to understand the properties of the clean system before examining the system with disorder. A thorough understanding of the properties of the clean system is required in order to be able to discern the effect of an added perturbation, in the form of a disorder potential, to the non-perturbed system.

The simulation results for the clean system are compared with the approximate analytical expression for the time-dependent axial density derived in Sec. 2.4. Throughout this section the physical constants a, t_1, e, and $\hbar$ are set equal to one. The electric field strength is thus expressed in these new units. A brief overview of the numerical method used to solve the model is given in Appendix C.

An initial state $\{c_k^j(0)\}$ is time evolved with the tight-binding Hamiltonian with an electrostatic coupling (Eq. (2.29)). The axial density is then calculated using the expression in Eq. (3.16). A half-filled band and a quarter-filled band are simulated. The system size is set to $L = 120$ sites in each case, unless otherwise stated. This choice of the number of sites is motivated by the fact that it is then possible to have an equal number of left-handed and right-handed electrons at the initial time, at both degrees of filling, in accordance with the Nielsen-Ninomiya theorem [1, 23]. For each degree of filling, three different values of the electric field strength are considered, $E = 0.05$, $E = 0.1$, and $E = 1$, respectively. The simulation results are shown in Fig. 3.1. The shape of the graph of the numerical solution and the amplitude of the numerical curve correspond well with the approximate analytical solution when $E = 1$. At the two lower field strengths, however, the amplitude of the numerical curve deviates from that of the analytical curve. These features hold at both degrees of filling. Another visible trait of the numerical solution is that the plateaux of the curve for a quarter-filled band are not smooth like the analytical solution. The electron density, $n(t)$, is naturally conserved in all cases.

In order to understand why the amplitude of the numerical solution depends on the electric field strength the former is plotted against varying electric field strength. This is done for three different fixed system sizes at both degrees of filling. The results from these simulations are shown in Fig. 3.2 (a)-(b). The amplitude tends towards the approximate analytical value as the field strength increases. The correspondence with the analytical case seems to be better with increasing system size. (The dip of the curves at $E \sim 0.2$, most prominent in Fig. 3.2 (b), is most likely due to a numerical artefact.) These characteristics hold for both degrees of filling.

The dependence of the numerical amplitude on the electric field strength and the system size can be understood by considering the two relevant time scales at hand. First, there is the time it takes for an electron to cross the system in the absence of an external electric field:

$$\tau_{sys} = \frac{L}{v_F}, \tag{3.17}$$

where v_F denotes the Fermi velocity, which is approximately equal to the average electron velocity. The other relevant time scale is the time it takes for an electron to complete a Bloch cycle:

$$\tau_B = \frac{2\pi\hbar}{eEa}. \tag{3.18}$$

If the time it takes for an electron to cross the system is less than the Bloch period, i.e. if $\tau_{sys} < \tau_B$, then the electron will be scattered against the boundaries of the system before it has been able to complete a Bloch cycle. The scattering of the electron(s) takes place since the electric field is incorporated in the Hamiltonian in Eq. (2.29) in such a way that the field is discontinuous at the boundary of the system. This will give rise to boundary scattering effects (even in the presence of periodic boundary conditions) which will reduce the amplitude of the graph of $n_5(t)$. The requirement that has to be met in order to see the whole amplitude is thus that the Bloch period is significantly smaller than the time it takes for the electron(s) to cross the system in the absence of an external field, i.e. $\tau_B \ll \tau_{sys}$, so that the electron(s) is able perform many oscillations before being scattered against the boundaries of the system. This implies that the electric field strength and the system size must be chosen sufficiently large, as can be seen by a direct comparison of the two time scales in Eqs. (3.17) and (3.18). Note that the comparison of the two time scales τ_B and τ_{sys} is valid only for a rough estimate of orders.

Another, equivalent, way of explaining the dependence of the amplitude on the electric field strength and the system size is to consider the two relevant energy scales at hand. First, there is the kinetic energy due to electron tunneling, $\epsilon_{tb} = t_1$. Second, there is the electrostatic energy, $\epsilon_{el} = eEa$. In the limit of large electric field strengths the kinetic energy is much smaller than the electrostatic energy, i.e. $t_1 \ll eEa$, such that the bare Hamiltonian, $\hat{H}_{tb}$, in Eq. (2.29) becomes very small compared to the electrostatic coupling, $\hat{V}_{el}$. The former can therefore be neglected to good approximation. In this regime the electrons perform "perfect Bloch oscillations" since the electron hopping can effectively be neglected. The correspondence with the approximate analytical solution will be very good in this case, since the analytical expression does not take into account the tunneling effect of the electrons. In the limit of small electric field strengths, the electrostatic coupling in Eq. (2.29) can be neglected to good approximation. In this limit the Bloch oscillations vanish and the only motion performed by the electrons is the hopping between lattice sites. There is then no effect that pumps electrons from left-handed to right-handed ones (or vice versa), and consequently, there will be no axial current. The regime $10^{-2} \lesssim E \lesssim 10^{-1}$ is a crossover regime, where tunneling effects can no longer be neglected. In this regime the term $\hat{H}_{tb}$ in Eq. (2.29) cannot be neglected; its effect is to dampen the Bloch oscillations.

As concerns the unevenness of the plateaux at the two lower field strengths in Fig. 3.1 it is probably due to boundary scattering effects. Boundary scattering effects will be present as long as the condition $\tau_B \ll \tau_{sys}$ is not satisfied. This is confirmed by plotting the axial density at quarter-filling for various system sizes, at the two lower field strengths (see Fig. 3.2 (c)-(d)).

Figure 3.3 shows the time evolution of the axial density in the limit of small electric field strengths. The curves in Fig. 3.3 do not have the same simple triangle-wave structure as does the corresponding curves in Fig. 3.1. This can partly be explained by boundary scattering effects. The wiggliness of the curves in Fig. 3.3 is probably due to the tunneling effect of the electrons, which becomes more pronounced at low field strengths.

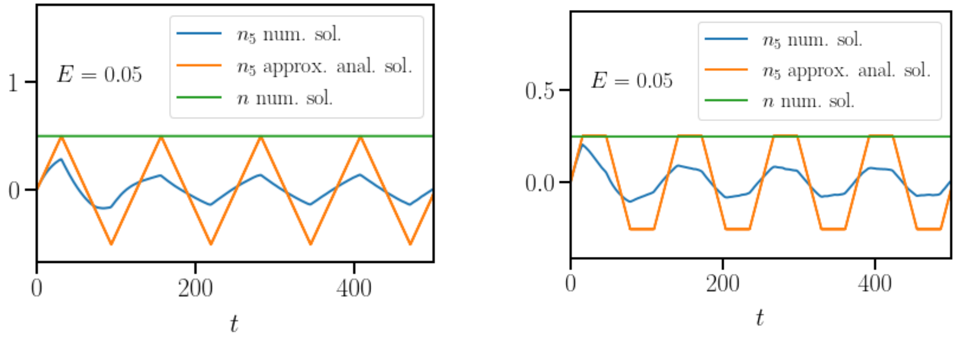

(a) Half-filling.

(b) Quarter-filling.

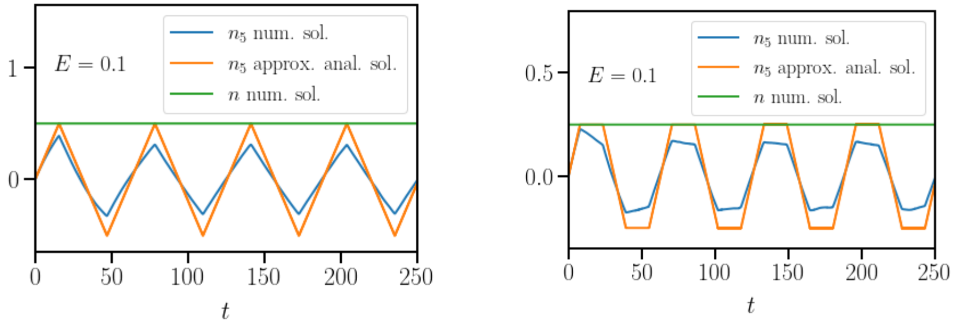

(c) Half-filling.

(d) Quarter-filling.

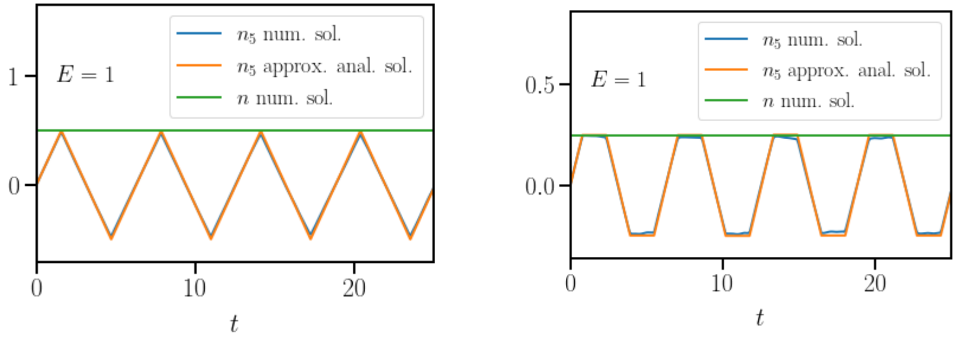

(e) Half-filling.

(f) Quarter-filling.

Figure 3.1: The axial density, n_5, as a function of time, t. The electric field strength $E = 0.05$ in Fig. (a)-(b), in Fig. (c)-(d) the field strength $E = 0.1$, and in Fig. (e)-(f) the field strength $E = 1$. The green line shows the electron density, n, as a function of time. "Approx. anal. sol." refers to Eqs. (2.32)-(2.38).

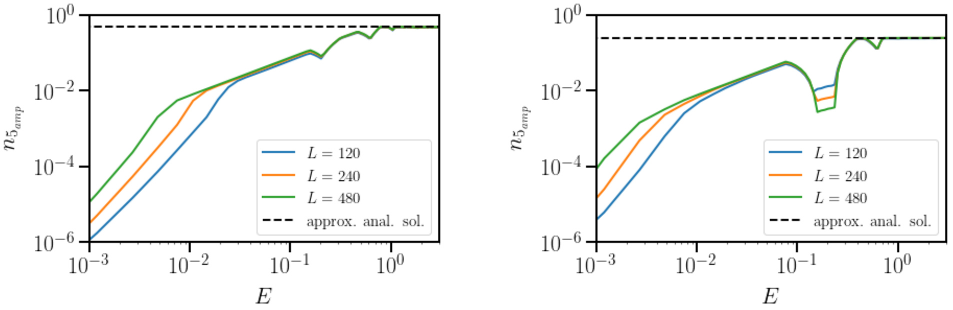

(a) Half-filling.

(b) Quarter-filling.

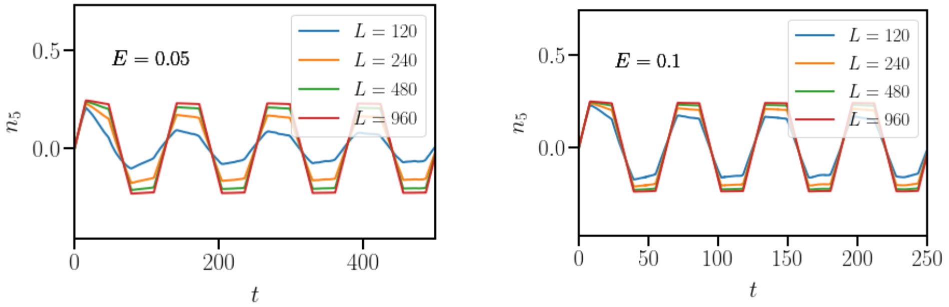

(c) $E = 0.05$, quarter-filling.

(d) $E = 0.1$, quarter-filling.

Figure 3.2: In Fig. (a) and (b) the amplitude of the axial density, $n_5(t)$, is plotted as a function of the electric field strength, E. Both axes are in logarithmic scale. (The dip of the curves at $E \sim 0.2$, most prominent in Fig. (b), is most likely due to a numerical artefact.) Figure (c) and (d) show the dependence on the system size of the axial density at quarter-filling for the two lower field strengths in Fig. 3.1, $E = 0.05$ and $E = 0.1$, respectively.

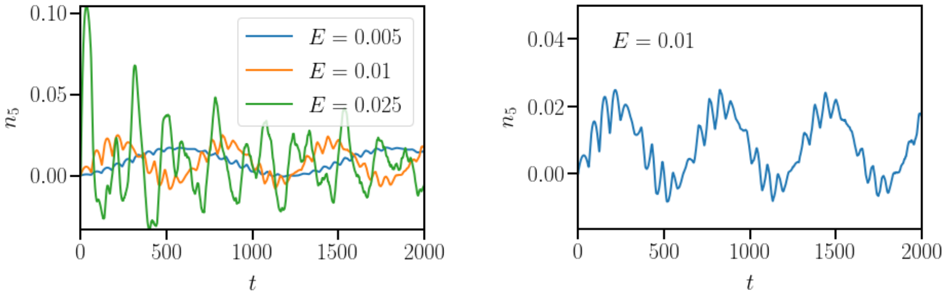

(a) Half-filling. (b) Half-filling.

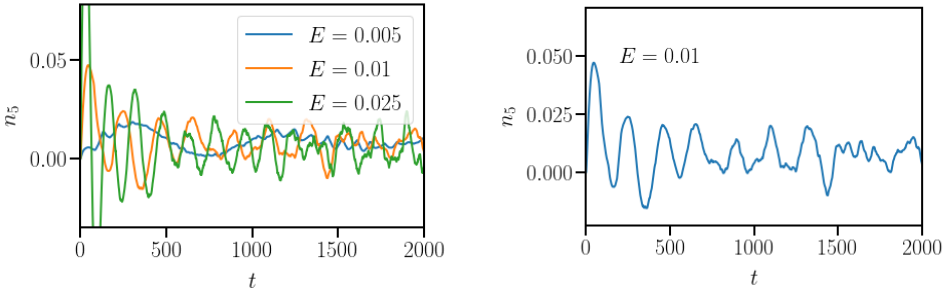

(c) Quarter-filling. (d) Quarter-filling.

Figure 3.3: The axial density, n_5, as a function of time, t, in the limit of small electric field strengths (relative to the hopping parameter, i.e. $eEa/t_1 \ll 1$). The reason that the form and amplitude of $n_5(t)$ deviates significantly from the approximate form in Eqs. (2.32)-(2.38) is that when $eEa/t_1 \ll 1$ the electrical field term in the Hamiltonian, which is the driver of the Bloch oscillations and the axial anomaly physics, is no longer the dominating term. In the left hand column (i.e. Figs. (a) and (c)) the effect on $n_5(t)$ of varying the electric field is shown and in the right hand column (i.e. Figs. (b) and (d)) $n_5(t)$ with $E = 0.01$ is shown again, for clarity.

Chapter 4

The disordered system

The disordered system, described by the Hamiltonian

$$\hat{H} = \hat{H}_{tb} + \hat{V}_{el} + \hat{V}_d, \tag{4.1}$$

with the disorder potential, $\hat{V}_d$, specified in Sec. 4.1, aims to give a description of the dynamics of spinless relativistic electrons in a crystalline potential, which is slightly perturbed by a random disorder potential $V(x)$. The disorder potential models the impurities in the crystal sample, i.e. the lattice imperfections, which will cause the electrons to scatter, and hence reduce the coherence of the Bloch oscillations.

4.1 The disorder potential

Formally, disorder is included in the tight-binding model by adding a term

$$\hat{V}_d = \sum_i V(x_i)\hat{c}_i^\dagger \hat{c}_i \tag{4.2}$$

to the right-hand side of Eq. (2.29). The function $V(x)$ is assumed to follow a random Gaussian distribution defined by its first two moments [11]:

$$\langle\!\langle V(x) \rangle\!\rangle = 0 \tag{4.3}$$

$$\langle\!\langle V(x)V(x') \rangle\!\rangle = f(x - x'), \tag{4.4}$$

where $\langle\!\langle \cdot \rangle\!\rangle$ denotes disorder average. Note that the statistical properties of the disorder potential are translation-invariant since averaging over disorder restores translation invariance (which is strongly broken for each disorder realisation considered) [11]. It is common to approximate the function f in Eq. (4.4) as a Dirac delta function. However, since the Fourier transform of the Dirac delta function is a constant, this implies that the potential $V(x)$ would scatter with any momentum transfer with the same probability. A more smooth potential that does not vary quickly on the scale of the lattice spacing is conveniently modeled by choosing f as a Gaussian [11, 24]:

$$f(x-x') = f_0 \exp\left[-\frac{(x-x')^2}{2\xi^2}\right]. \tag{4.5}$$

By the rescaling

$$f_0 \to t_1^2 \frac{a}{\sqrt{2\pi}\xi} f_0, \tag{4.6}$$

the prefactor in Eq. (4.5) is made dimensionless. The inclusion of the tunneling amplitude in the prefactor has no physical significance for the disorder. The tunneling amplitude is used in the rescaling of the prefactor only to get correct dimension. In the simulations t_1 is set to one. The two-point correlator becomes

$$\langle\!\langle V(x)V(x')\rangle\!\rangle = f_0 t_1^2 \frac{a}{\sqrt{2\pi}\xi} \exp\left[-\frac{(x-x')^2}{2\xi^2}\right], \tag{4.7}$$

where f_0 is the dimensionless correlation strength, and ξ is the correlation length.

To generate a potential function $V(x)$ with the properties defined above, start to consider the Fourier expansion of $V(x)$:

$$V(x) = \frac{1}{\sqrt{L}} \sum_n V_{q_n} e^{iq_n x}, \qquad q_n = \frac{2\pi n}{L} \quad n \in \mathbb{Z}, \tag{4.8}$$

where

$$V_{q_n} = \frac{1}{\sqrt{L}} \int_0^L V(x) e^{-iq_n x}\, dx. \tag{4.9}$$

Note that since $V(x)$ is real-valued it follows that the Fourier coefficients, V_q, satisfy $V_{-q} = V_q^*$. By inserting the Fourier expansion of $V(x)$ into Eq. (4.4) and using the properties of $V(x)$ it follows that the only non-zero correlator for the Fourier components is given by

$$\langle\!\langle |V_{q_n}|^2 \rangle\!\rangle = f_0 t_1^2 a e^{-\xi^2 q_n^2/2} \equiv \sigma_{q_n}^2. \tag{4.10}$$

For details see Appendix D. The V_{q_n} are independently distributed for different q_n and have variance $\sigma_{q_n}^2$. Note that Eq. (4.10) only determines $|V_q|^2$ and not V_q. The latter has a random phase

$$V_q = |V_q| e^{i\phi_q}, \tag{4.11}$$

where $|V_q|$ is normal distributed with standard deviation $\sigma_q = \sqrt{f_0 a} t_1 e^{-\xi^2 q^2/4}$, and, since $|V_q| > 0$, the negative values in the distribution $\mathcal{N}(0, \sigma_q)$ are discarded. The disorder potential in real space is given by

$$V(x) = \frac{2}{\sqrt{L}} \sum_{n>0} |V_{q_n}| \cos(q_n x + \phi_{q_n}). \tag{4.12}$$

The Fourier transform of Eq. (4.2) is furthermore given by

$$\hat{V}_d = \sum_{k,k'} V_{d_{k,k'}} \hat{c}_k^\dagger \hat{c}_{k'}, \tag{4.13}$$

where

$$V_{d_{k,k'}} = \begin{cases} \frac{1}{\sqrt{L}} |V_{|k-k'|}| e^{\operatorname{sgn}(k-k') i\phi_{|k-k'|}} & k \neq k' \\ 0 & k = k'. \end{cases} \tag{4.14}$$

4.2 Scattering rate

The rate at which right-moving electrons are scattered to left-moving ones (or vice versa) due to the disorder potential is given by

$$\frac{N_5}{\tau} = \sum_k \sum_{k'} \Gamma_{k\to k'} f(k)(1 - f(k')), \tag{4.15}$$

where $f(k)$ is an occupation function defined as

$$f(k) = \begin{cases} 1 & \text{if the state with wave vector } k \text{ is occupied,} \\ 0 & \text{otherwise.} \end{cases} \tag{4.16}$$

The inclusion of the factors of f in the expression for the scattering rate ensures that an electron can only scatter to an unoccupied state, in accordance with the Pauli exclusion principle. The wave vector corresponding to the rightmost occupied state in the band is k_+, and the wave vector corresponding to the leftmost occupied state, for which an electron is free to scatter to the opposite side of the band, is k_-. The transition rate $\Gamma_{k\to k'}$ is given by Fermi's golden rule [11, 22]:

$$\Gamma_{k\to k'} = \frac{2\pi}{\hbar} \langle\!\langle | \langle \phi_{k'} | \hat{V}_d | \phi_k \rangle |^2 \rangle\!\rangle \delta(\epsilon_{k'} - \epsilon_k). \tag{4.17}$$

An electron in the crystal is scattered from one Bloch state to another [22]. The initial and final states in Eq. (4.17) are given by

$$\phi_k = \frac{1}{\sqrt{L}} e^{ikx}, \qquad \phi_{k'} = \frac{1}{\sqrt{L}} e^{ik'x}, \tag{4.18}$$

with corresponding energies given by Eq. (2.11). This assumes however that the electric field strength is relatively weak, i.e. small compared to the tunneling amplitude, $E \ll t_1$. The matrix element in Eq. (4.17) is given by

$$\langle \phi_{k'} | \hat{V}_d | \phi_k \rangle = \int \phi_{k'}^* \hat{V}_d \phi_k \, dx = \frac{1}{L} \int V_d(x) e^{-i(k'-k)x} \, dx = \frac{1}{\sqrt{L}} V_d(k' - k). \tag{4.19}$$

The scattering rate becomes

$$\begin{aligned}
\frac{N_5}{\tau} &= \sum_k \sum_{k'} \frac{2\pi}{\hbar} \langle\!\langle |\langle \phi_{k'}|\hat{V}_d|\phi_k\rangle|^2 \rangle\!\rangle \delta(\epsilon_{k'} - \epsilon_k) f(k)(1 - f(k')) \qquad (4.20)\\
&= \left(\frac{L}{2\pi}\right)^2 \iint \frac{2\pi}{\hbar}\frac{1}{L} \langle\!\langle |V_d(k'-k)|^2 \rangle\!\rangle \delta(\epsilon_{k'} - \epsilon_k) f(k)(1 - f(k'))\, dk dk'\\
&= \frac{L}{2\pi\hbar} \iint \langle\!\langle |V_d(k'-k)|^2 \rangle\!\rangle \frac{\delta(k'+k)}{2t_1 a|\sin(ka)|} f(k)(1 - f(k'))\, dk dk'\\
&= \frac{L}{4\pi\hbar t_1 a} \int_{-\pi/a}^{\pi/a} dk \frac{\langle\!\langle |V_d(2k)|^2 \rangle\!\rangle}{|\sin(ka)|} f(k)(1 - f(-k))\\
&= \frac{L}{4\pi\hbar t_1 a} \int_{k_-}^{k_+} dk \frac{\langle\!\langle |V_d(2k)|^2 \rangle\!\rangle}{|\sin(ka)|}\\
&\simeq \frac{L}{4\pi\hbar t_1 a} \frac{\langle\!\langle |V_d(2k_F^+)|^2 \rangle\!\rangle}{\sin(k_F^+ a)} \Delta k,
\end{aligned}$$

where the approximation on the last line assumes that n_5 is small (and that $k_F^+ \in [k_-, k_+]$). The assumption that n_5 is small, i.e. $n_5 \ll 1$, makes it possible to approximate k_F^+ as $k_F^+ \sim k_F^+(0) = \pi/2a$ at half-filling. The number of states in the interval Δk is per definition equal to the number of chiral particles in the system,

$$N_5 \equiv \frac{\Delta k}{2\pi/L}. \qquad (4.21)$$

Insertion of this in the expression for the scattering rate gives

$$\frac{N_5}{\tau} \simeq \frac{\langle\!\langle |V_d(2k_F^+)|^2 \rangle\!\rangle}{2\hbar t_1 a \sin(k_F^+ a)} N_5, \qquad (4.22)$$

whence

$$\tau \simeq \frac{2\hbar \sin(k_F^+ a) e^{2\xi^2 (k_F^+)^2}}{f_0 t_1}. \qquad (4.23)$$

It is probably possible to improve on the approximations used to compute the integral in Eq. (4.20), however this will only alter the k_F-dependence in τ in Eq. (4.23) and most likely only produce minor corrections.

4.3 Energy scales

In the clean limit there are two energy scales present, $\epsilon_{tb} = t_1$ and $\epsilon_{el} = eEa$, respectively. This corresponds to one effective energy scale eEa/t_1. In this case, there are three limiting cases to consider

$$eEa/t_1 \ll 1, \qquad eEa/t_1 \sim 1, \qquad eEa/t_1 \gg 1. \qquad (4.24)$$

These cases were all accounted for in Sec. 3.3. The inclusion of disorder adds a new energy scale, ϵ_{dis}, whose magnitude follows from the two-point correlator in Eq. (4.8):

$$\epsilon_{dis} \sim \sqrt{\frac{f_0 a}{\sqrt{2\pi}\xi}} t_1. \tag{4.25}$$

When $E = 0$, there are three limiting cases

$$\epsilon_{dis}/t_1 \ll 1, \qquad \epsilon_{dis}/t_1 \sim 1, \qquad \epsilon_{dis}/t_1 \gg 1, \tag{4.26}$$

and when the electric field is turned on there are thus $3 \cdot 3 = 9$ limiting cases to consider. To this comes the parameter ξ, the correlation length, which is not an energy, but still a free parameter in the system to consider. There are two limiting cases pertaining to this parameter:

$$\xi \lesssim a \quad \text{(short-range)}, \qquad \xi \gg a \quad \text{(long-range)}. \tag{4.27}$$

It follows that there are $2 \cdot 3 \cdot 3 = 18$ limiting cases to consider for the disordered system. It will however not be possible to cover all of the cases in this work. The focus will be on examining the limits in Eq. (4.26), for short-ranged and long-ranged correlations, and weak electric field strengths.

4.4 Numerical results

A system with $L = 120$ sites is simulated at half-filling and quarter-filling. The electric field strength is set to $E = 0.01$. This corresponds to a weak electric field compared to the kinetic energy scale, i.e. $\epsilon_{el} < \epsilon_{tb}$, but a relatively large field to produce in a lab (see Appendix E). The numerically computed axial density, $n_5(t)$, is compared with the semiclassical expression in Eq. (2.45). The comparison with the numerical result is done both using the estimate for the scattering time calculated within the Fermi golden rule (FG) approximation (Eq. (4.23)), and by a curve fitting routine, where the optimal values of the scattering time τ and the steady state value of $n_5(t)$ are calculated from the simulation data and fitted to the target function (Eq. (2.45)).

Figure 4.1 and 4.2 show the time evolution of the axial density in the various regimes of disorder given in Eq. (4.26). Both short-ranged and long-ranged correlations are considered. Short-ranged correlations give results that correspond well with Eq. (2.45). In this case, the numerical solution saturates at a non-zero value at both degrees of filling, thus indicating the absence of Anderson localization. This is the expected behaviour in the regime of strong disorder, since the scattering induced by disorder obstructs the pumping mechanism of the electric field, which leads to a non-equilibrium steady state with non-zero axial density [9]. Note however that Eq. (2.45) with the scattering time τ calculated within the FG approximation is not a good approximation to the numerical curve at weak to moderate short-ranged disorder.

Weak to moderate disorder with long-range correlations give results that resemble the clean limit at both degrees of filling (Compare Fig. 4.1 (b) and (d) with Fig. 3.3 (b), and Fig. 4.2 (b) and (d) with Fig. 3.3 (d), respectively.). At strong disorder with long-range correlations the numerical solution saturates at a non-zero value. Equation (2.45) with the scattering time calculated within the FG approximation overestimates the numerical solution in case of long-range correlations. The simulation results for the field strengths $E = 0.001$ and $E = 0.05$ are similar to those for $E = 0.01$.

Possible reasons as to why the FG approximation breaks down in certain parameter regimes are that the assumptions made in the derivation of the FG approximation include a weak perturbation, i.e. a weak electric field and a weak disorder potential relative to the kinetic energy scale. It is also unlikely that the FG approximation can accurately account for correlations in space. However, the FG approximation actually is more accurate for strong disorder, i.e. large perturbations, which goes directly against the condition of validity.

Figure 4.3 shows the scattering time τ and the steady state value of $n_5(t)$ as a function of the disorder strength, f_0. The FG approximation (Eq. (4.23)) is plotted for comparison. Two different correlation lengths are considred, $\xi = 0.1$ and $\xi = 0.75$. The scattering time tends to zero as disorder increases, as is evident by looking at Eq. (4.23). The convergence is faster the smaller the correlation length. The analogous reasoning, of course, holds for the steady state value of $n_5(t)$, since it is directly proportional to the scattering time.

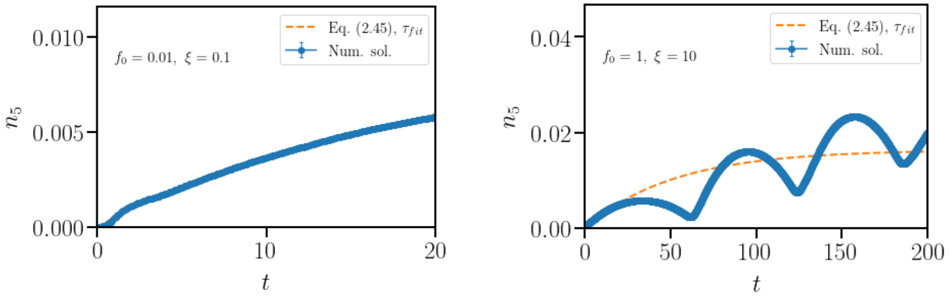

(a) Weak short-ranged disorder.

(b) Weak long-ranged disorder.

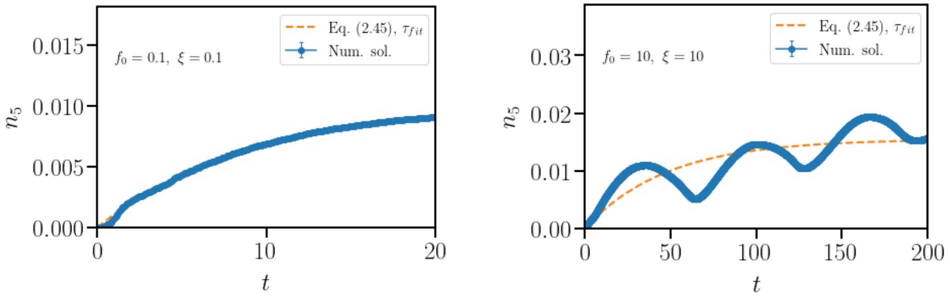

(c) Moderate short-ranged disorder.

(d) Moderate long-ranged disorder.

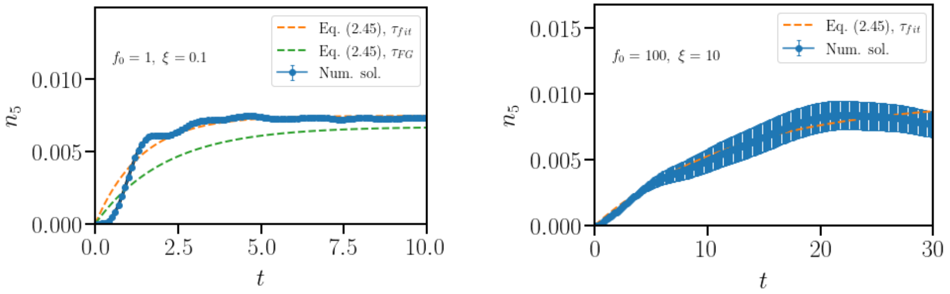

(e) Strong short-ranged disorder.

(f) Strong long-ranged disorder.

Figure 4.1: The axial density, n_5, as a function of time, t, at half-filling. The electric field strength $E = 0.01$. For (a)-(f), six different disorder regimes are considered. The numerical data is averaged over 1000 different disorder realisations in each case.

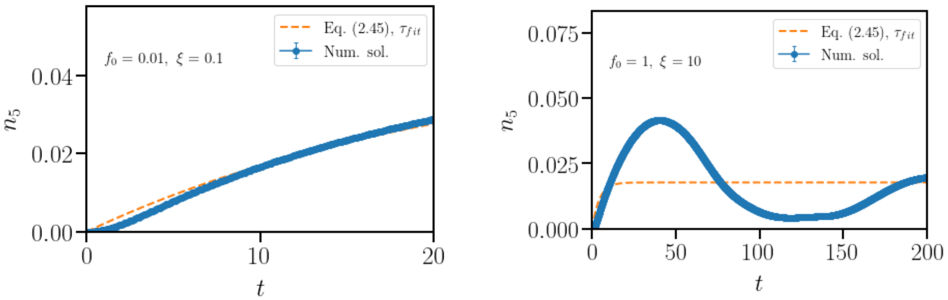

(a) Weak short-ranged disorder.

(b) Weak long-ranged disorder.

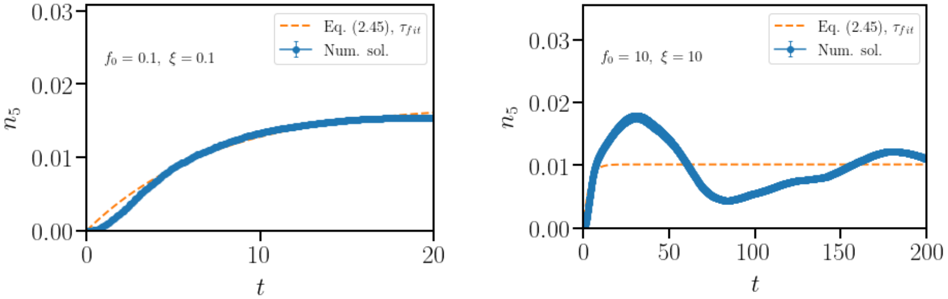

(c) Moderate short-ranged disorder.

(d) Moderate long-ranged disorder.

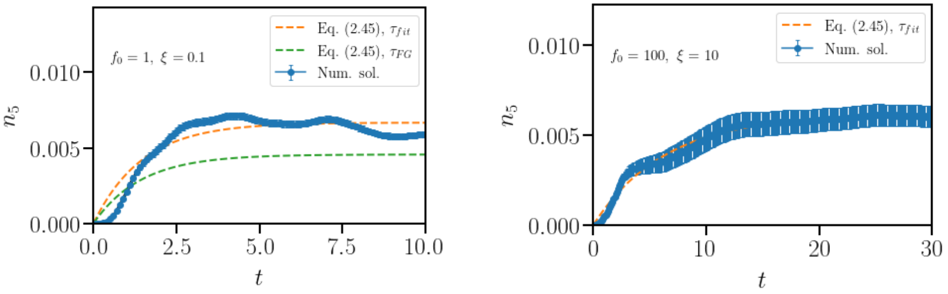

(e) Strong short-ranged disorder.

(f) Strong long-ranged disorder.

Figure 4.2: The axial density, n_5, as a function of time, t, at quarter-filling. The electric field strength $E = 0.01$. For (a)-(f), six different disorder regimes are considered. The numerical data is averaged over 1000 different disorder realisations in each case.

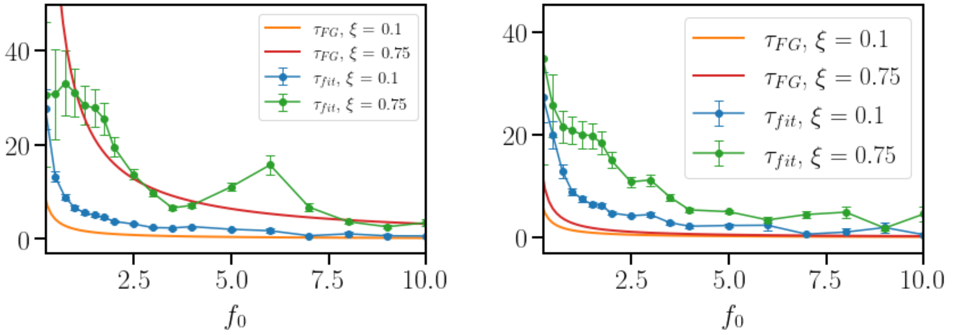

(a) Half-filling. (b) Quarter-filling.

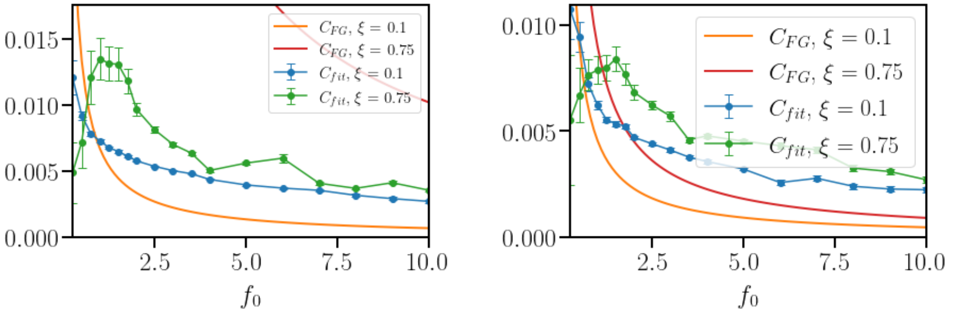

(c) Half-filling. (d) Quarter-filling.

Figure 4.3: In Fig. (a) and (b) the scattering time, τ, is plotted versus the disorder strength, f_0, for two different values of the correlation length, $\xi = 0.1$ and $\xi = 0.75$. The Fermi golden rule (FG) approximation (Eq. (4.23)) is plotted for comparison. In Fig. (c)-(d) the steady state value of $n_5(t)$, $C = eE\tau/\pi\hbar$, is plotted versus f_0. The electric field strength $E = 0.01$.

Chapter 5

Conclusion

This study has investigated the effect of disorder on the time-dependent signature of the axial anomaly in a one-band tight-binding model in one spatial dimension. The model system consists of a one-dimensional monatomic crystal with spinless electrons which disperse linearly in certain regions of reciprocal space, thus corresponding to electrons in the massless limit in these regions. The electrons are accelerated by a static and uniform electric field which gives rise to Bloch oscillations. The Bloch oscillations can, in the case of linearly dispersing electrons, be viewed as a transfer of electrons with a given chirality (e.g. right-handed) to a state with the opposite chirality (left-handed). The result is an alternating current of axial particles (electrons), and hence the non-conservation of the axial density, $n_5(t)$.

An approximate analytical expression for the time-dependent axial density, $n_5(t)$, has been derived in the absence of an external disorder potential. The correspondence between the approximate analytical expression for $n_5(t)$ and the numerical solution of the tight-binding model without disorder appeared to be better the larger the electric field strength and the system size used in the simulations. This feature can be explained by comparing the two relevant time scales for the clean system. The simulation results for the non-perturbed system also showed that boundary scattering and tunneling effects become prominent in the limit of weak electric field strengths.

In order to examine the effect of disorder on the system, a disorder potential with Gaussian correlations was implemented in the tight-binding model. Both long-range and short-range correlations were considered in the solution of the disordered model. The numerical solution of the disordered model was compared with a semiclassical expression for the time-dependent axial density in the presence of disorder, a result due to Nielsen and Ninomiya [1]. The correspondence between the numerical solution and the semiclassical expression appeared to be good in all parameter regimes considered, except for weak to moderate disorder and long-range correlations.

The scattering time of the electron(s) due to disorder was estimated using Fermi's golden rule. The FG approximation showed to be more accurate for large perturbations, i.e. strong disorder, than for weak perturbations, in contrast with the validity condition of the FG approximation. There is no obvious reason as to why the FG approximation should be more accurate for a strongly perturbed system than for a weakly perturbed system.

For future work it would be interesting to try to extend the one-dimensional model here presented to a three-dimensional setting in order to achieve a model that more accurately mimics the essential features of a Weyl semimetal. This would require the inclusion of a magnetic field in the tight-binding model [1], and one would have to find some tractable way to deal with the numerical solution of the model, since this calculation would be a lot heavier than its counterpart in $1 + 1$ dimensions. It would be interesting to see if the $(1 + 1)$-dimensional model and the $(3 + 1)$-dimensional model give similar results or if they differ in any vital aspect. It would also be rewarding to compare the numerical result with experimental values for Weyl semimetals.

Appendices

Appendix A

A formula for the axial density in terms of expansion coefficients

To obtain an analytical expression for the axial density of a multi-electron system in terms of the expansion coefficients $c_k(t)$ (see Eq. (3.5)) one can proceed in the following way. First, a many-body state, which fulfils the Pauli exclusion principle, is constructed. The expectation value of a generic one-body operator, $\hat{\mathcal{O}}$, given by the sum of single-particle operators, $\hat{\mathcal{O}}_j$,

$$\hat{\mathcal{O}} = \sum_j \hat{\mathcal{O}}_j, \tag{A.1}$$

is then calculated, where the single-particle operator $\hat{\mathcal{O}}_j$ acts on the jth particle in the system. The axial density for the multi-electron system is obtained by replacing the operator $\hat{\mathcal{O}}$ by the total axial density operator, $\sum_j \hat{n}_{5,j}$, in this calculation.

Consider a product state of N single-particle states $|\phi_1\rangle \ldots |\phi_N\rangle$

$$|\phi_1\rangle \otimes \ldots \otimes |\phi_N\rangle \,. \tag{A.2}$$

Define the anti-symmetrized many-body state as

$$|\phi_1, \ldots, \phi_N\rangle_- \equiv \hat{A}\, |\phi_1\rangle \otimes \ldots \otimes |\phi_N\rangle \,, \tag{A.3}$$

where $\hat{A}$ is the anti-symmetrizing operator given by

$$\hat{A} \equiv \frac{1}{N!} \sum_p \mathrm{sgn}(p) \hat{P}_p. \tag{A.4}$$

The normalized anti-symmetrized many-body state is given by

$$|\phi_1, ..., \phi_N\rangle_- = \frac{1}{\sqrt{N!}} \sum_p \text{sgn}(p) \hat{P}_p \, |\phi_1\rangle \otimes ... \otimes |\phi_N\rangle \,. \tag{A.5}$$

Notice that an arbitrary single-particle operator in the definition of $\hat{\mathcal{O}}$ can be written as

$$\hat{\mathcal{O}}_j = \mathbb{1} \otimes ... \otimes \mathbb{1} \otimes \underbrace{\hat{\mathcal{O}}_1}_{j^{\text{th}} \text{ place}} \otimes \mathbb{1} \otimes ... \otimes \mathbb{1}, \tag{A.6}$$

where $\hat{\mathcal{O}}_1$ is a single-particle operator that acts on the jth particle in the system. The expectation value of the operator $\hat{\mathcal{O}}$ is given by

$$\begin{aligned}
\langle \hat{\mathcal{O}} \rangle &= \left\langle \phi_1, ..., \phi_N \,\middle|\, \hat{\mathcal{O}} \,\middle|\, \phi_1, ..., \phi_N \right\rangle \qquad \text{(A.7)} \\
&= \frac{1}{N!} \sum_j \sum_{p,p'} \text{sgn}(p)\text{sgn}(p') \left\langle \phi_{p_1} | \phi_{p'_1} \right\rangle ... \left\langle \phi_{p_j} \middle| \hat{\mathcal{O}}_1 \middle| \phi_{p'_j} \right\rangle ... \left\langle \phi_{p_N} | \phi_{p'_N} \right\rangle \\
&= \frac{1}{N!} \sum_j \sum_{p,p'} \text{sgn}(p)\text{sgn}(p') \delta_{p,p'} \left\langle \phi_{p_j} \middle| \hat{\mathcal{O}}_1 \middle| \phi_{p'_j} \right\rangle \\
&= \frac{1}{N!} \sum_p \sum_j \left\langle \phi_{p_j} | \hat{\mathcal{O}}_1 | \phi_{p_j} \right\rangle \\
&= \sum_j \left\langle \phi_j | \hat{\mathcal{O}}_1 | \phi_j \right\rangle .
\end{aligned}$$

The expectation value of a generic one-body operator, $\hat{\mathcal{O}}$, given by the sum of single-particle operators, $\hat{\mathcal{O}}_j$, is thus given by the sum of the expectation values of the single-particle operators which act on the individual particles in the system. This implies that the axial density for the multi-electron system is given by the sum of the axial densities for the individual electrons in the system, i.e.

$$n_5(t) = \sum_j n_5^j(t) = \frac{1}{L} \sum_j \Big(\sum_{k>0} |c_k^j(t)|^2 - \sum_{k<0} |c_k^j(t)|^2 \Big), \tag{A.8}$$

where the initial state $\{n_5^j(0)\}$ is different for different particles in order to fulfil the Pauli exclusion principle. Equation (A.8) holds during time evolution since a product state time evolved with a non-interacting Hamiltonian remains a product state (see Appendix B).

Appendix B

Time evolution of a product state with a non-interacting Hamiltonian

In this appendix the time evolution of a product state with a non-interacting Hamiltonian is considered. It is shown that the state remains a product state after time evolution. What follows is based on chapter 10 in Shankar's book [25] and chapter 8 in the book by Zettili [26].

A product state is a separable state of the form

$$\alpha = \alpha_1 \otimes \alpha_2, \tag{B.1}$$

where α_1 and α_2 are states which belong to subsystem 1 and 2, respectively. This definition can be generalized to an arbitrary number of subsystems. A non-interacting Hamiltonian can be written as a sum of the individual Hamiltonians that constitute the joint system

$$\hat{H} = \sum_i \hat{H}_i, \tag{B.2}$$

where $\hat{H}_i$ is the Hamiltonian of the ith subsystem. The Schrödinger Hamiltonian of a system of N non-interacting distinguishable particles is given by

$$\hat{H} = \sum_{i=1}^{N} \left[\frac{\hat{p}_i^2}{2m_i} + V_i(\hat{x}_i) \right], \tag{B.3}$$

where $\hat{x}_i$ and $\hat{p}_i$ are the position and momentum operators of the ith particle, and the external potential V_i acts on the ith particle in the system.

To begin with, a system of two non-interacting distinguishable particles is considered. The time-evolved state is then anti-symmetrized to take into account indistinguishability. It is straightforward to generalize the result to a system of arbitrary size.

The Schrödinger Hamiltonian of a system of two non-interacting particles is given by

$$\hat{H} = \hat{H}_1 + \hat{H}_2 = \frac{\hat{p}_1^2}{2m_1} + V_1(\hat{x}_1) + \frac{\hat{p}_2^2}{2m_2} + V_2(\hat{x}_2), \tag{B.4}$$

where $\hat{x}_i$ and $\hat{p}_i$ are the position and momentum operators acting on particle i ($i = 1, 2$). The Hilbert space of the joint system is given by the direct product of the separate Hilbert spaces of the two particles

$$\mathscr{H}_{1\otimes 2} = \mathscr{H}_1 \otimes \mathscr{H}_2. \tag{B.5}$$

The state vector of the two-particle system is an element of the Hilbert space of the joint system and it evolves in time according to the Schrödinger equation

$$i\hbar \frac{\partial \left|\psi(t)\right\rangle}{\partial t} = (\hat{H}_1 + \hat{H}_2) \left|\psi(t)\right\rangle = \hat{H} \left|\psi(t)\right\rangle. \tag{B.6}$$

The solution to Eq. (B.6) with $\hat{H}$ given by Eq. (B.4) is a stationary state

$$\left|\psi(t)\right\rangle = \left|E\right\rangle e^{-iEt/\hbar}, \tag{B.7}$$

where E is the total energy of the joint system. Equation (B.6) can thus be reduced to its time-independent version

$$(\hat{H}_1 + \hat{H}_2) \left|E\right\rangle = E \left|E\right\rangle. \tag{B.8}$$

The single-particle Hamiltonians, $\hat{H}_1$ and $\hat{H}_2$, commute and it is therefore possible to find their simultaneous eigenstates. These are given by

$$\left|E_1 E_2\right\rangle = \sum_n c_n \left|E_{1,n}\right\rangle \otimes \sum_m c_m \left|E_{2,m}\right\rangle, \tag{B.9}$$

where $\left|E_{1,n}\right\rangle$ and $\left|E_{2,m}\right\rangle$ are solutions to the time-independent Schrödinger equation of the respective subsystem

$$\hat{H}_1 \left|E_{1,n}\right\rangle = E_{1,n} \left|E_{1,n}\right\rangle \tag{B.10}$$

$$\hat{H}_2 \left|E_{2,m}\right\rangle = E_{2,m} \left|E_{2,m}\right\rangle. \tag{B.11}$$

Consider the action of $\hat{H}$ on an energy eigenstate $\left|E\right\rangle$ of the joint system

$$\hat{H} \left|E\right\rangle = (\hat{H}_1 + \hat{H}_2) \left|E_1 E_2\right\rangle = (E_{1,n} + E_{2,m}) \left|E_1 E_2\right\rangle = (E_{1,n} + E_{2,m}) \left|E\right\rangle. \tag{B.12}$$

This implies that the total energy of the joint system is given by the sum of the single-particle eigenenergies $E_{1,n}$ and $E_{2,m}$, i.e.

$$E = E_{1,n} + E_{2,m}. \tag{B.13}$$

Substitution of Eqs. (B.9) and (B.13) into Eq. (B.7) yields the time evolved state of the joint system

$$|\psi(t)\rangle = \sum_n c_n \, |E_{1,n}\rangle \, e^{-iE_{1,n}t/\hbar} \otimes \sum_m c_m \, |E_{2,m}\rangle \, e^{-iE_{2,m}t/\hbar}, \tag{B.14}$$

which is a product state. The corresponding anti-symmetrized state is given by

$$|\psi(t)\rangle_A = \frac{1}{\sqrt{2}} \sum_{n,m} c_n c_m \big[\, |E_{1,n}\rangle \otimes |E_{2,m}\rangle - |E_{2,m}\rangle \otimes |E_{1,n}\rangle \,\big] e^{-i(E_{1,n}+E_{2,m})t/\hbar}. \tag{B.15}$$

For a system consisting of N non-interacting particles the anti-symmmetrized product state is given by

$$|\psi(t)\rangle_A = \frac{1}{\sqrt{N!}} \sum_{n,\ldots,l} c_n \cdots c_l \begin{vmatrix} |1:E_{1,n}\rangle & \cdots & |1:E_{N,l}\rangle \\ \vdots & \ddots & \vdots \\ |N:E_{1,n}\rangle & \cdots & |N:E_{N,l}\rangle \end{vmatrix} e^{-i(E_{1,n}+\ldots+E_{N,l})t/\hbar}, \tag{B.16}$$

where the determinant is called the Slater determinant.

Appendix C

Numerical method

The numerical method used to solve the Schrödinger equation in momentum space (Eq. (3.7)) is briefly described in this appendix. The first step is to define the matrix elements $H_{k,k'}$ in Python which is quite straightforward. The disorder part is implemented by generating random numbers $|V_{q_n}|$ from a normal distribution with zero mean and standard deviation given by Eq. (4.10). The $|V_{q_n}|$ are multiplied by a random phase, as indicated in Eq. (4.11), and added up to get the total disorder potential in momentum space. The following scheme is then used to time evolve an initial state $\{c_k^j(0)\}$:

1. Define an initial state $\{c_k^j(0)\}$ which fulfils the Pauli principle. This step corresponds to assigning different initial positions to different electrons in the system.

2. Calculate the unitary time evolution operator in momentum space

   $$U_{k,k'}(\Delta t) = (e^{-i\hat{H}\Delta t/\hbar})_{k,k'} \tag{C.1}$$

   for a suitably chosen time step Δt. The unitary time evolution operator is an exponential matrix for which there exists a predefined function in most programming languages.

3. In order to solve the system of ordinary differential equations in Eq. (3.7), act with the unitary time evolution operator on the initial state (in step [1])

repeatedly, as follows:

$$\begin{aligned} c_k(t_1 = \Delta t) &= \sum_{k'} U_{k,k'}(\Delta t) c_{k'}(0) \\ c_k(t_2 = 2\Delta t) &= \sum_{k'} U_{k,k'}(\Delta t) c_{k'}(\Delta t) \\ &\vdots \\ c_k(t_n = n\Delta t) &= \sum_{k'} U_{k,k'}(\Delta t) c_{k'}((n-1)\Delta t). \end{aligned}$$

> This is not the standard way of numerically integrating a system of ODEs (built-in integrators that are designed to handle both linear and nonlinear equations, like e.g. the Runge-Kutta method typically uses the finite difference approximation for approximating the derivative term). Here one exploits the fact that Eq. (3.7) is linear in $c_k(t)$, thus the general solution may be expressed in terms of the matrix exponential function (see any mathematical handbook for reference, e.g. [27]).

The time evolved state obtained in this way is then used to calculate the axial density for the whole system using the expression for $n_5(t)$ in Eq. (3.16).

In the case when the disorder potential is included in the Hamiltonian the procedure outlined above is simply iterated a given number of disorder realisations and as a last step disorder averages of the observables are computed.

Appendix D

The disorder potential

Insertion of the Fourier transform

$$V(x) = \frac{1}{\sqrt{L}} \sum_n V_{q_n} e^{iq_n x} \tag{D.1}$$

into the expression for the two-point correlator gives

$$\langle\!\langle V(x)V(x') \rangle\!\rangle = \frac{1}{L} \sum_{n,n'} \langle\!\langle V_{q_n} V_{q_{n'}} \rangle\!\rangle e^{iq_n x + iq_{n'} x'}. \tag{D.2}$$

The left-hand side of Eq. (D.2) depends only on $x - x'$. For this to hold also for the right-hand side let

$$\langle\!\langle V_{q_n} V_{q_{n'}} \rangle\!\rangle = F(q_n) \delta_{q_n, -q_{n'}}. \tag{D.3}$$

This gives

$$\langle\!\langle V(x)V(x') \rangle\!\rangle = f_0 t_1^2 \frac{a}{\sqrt{2\pi}\xi} \exp\left[-\frac{(x-x')^2}{2\xi^2} \right] = \frac{1}{L} \sum_n F(q_n) e^{iq_n (x-x')}. \tag{D.4}$$

To determine the function $F(q_n)$ both sides of Eq. (D.4) are multiplied with a factor $e^{-iq_m x}$ and integrated over the system. This gives

$$\begin{aligned} f_0 t_1^2 \frac{a}{\sqrt{2\pi}\xi} \int_0^L dx\, e^{-(x-x')^2/2\xi^2 - iq_m x} &= \\ \sum_n F(q_n) e^{-iq_n x'} \underbrace{\frac{1}{L} \int_0^L dx\, e^{i(q_n - q_m)x}}_{\delta_{q_n, q_m}}&, \end{aligned} \tag{D.5}$$

whence

$$F(q_m) e^{-iq_m x'} = f_0 t_1^2 \frac{a}{\sqrt{2\pi}\xi} \int_0^L dx\, e^{-(x-x')^2/2\xi^2 - iq_m x}. \tag{D.6}$$

Both sides of Eq. (D.6) are then multiplied by a factor $e^{iq_m x'}$, which gives

$$F(q_n) = f_0 t_1^2 \frac{a}{\sqrt{2\pi}\xi} \int_0^L dx\, e^{-(x-x')^2/2\xi^2 - iq_n(x-x')}, \tag{D.7}$$

where the integral

$$\int_0^L dx\, e^{-(x-x')^2/2\xi^2 - iq_m(x-x')} \simeq \int_{-\infty}^{\infty} dx\; e^{-x^2/2\xi^2 - iq_n x} = \sqrt{2\pi}\xi e^{-\xi^2 q_n^2/2}. \tag{D.8}$$

The function F is hence given by

$$F(q_n) \simeq f_0 t_1^2 a e^{-\xi^2 q_n^2/2}. \tag{D.9}$$

It follows that the only non-zero correlator for the Fourier components is

$$\langle\!\langle |V_{q_n}|^2 \rangle\!\rangle = f_0 t_1^2 a e^{-\xi^2 q_n^2/2}. \tag{D.10}$$

In order to write the disorder potential in real space, notice that

$$V_{-q} = |V_{-q}| e^{i\phi_{-q}} = (|V_q| e^{i\phi_q})^* = |V_q| e^{-i\phi_q} \quad \Rightarrow \tag{D.11}$$

$$|V_{-q}| = |V_q|, \qquad e^{i\phi_{-q}} = e^{-i\phi_q}. \tag{D.12}$$

Using the properties specified in Eqs. (D.11) and (D.12) one gets

$$\begin{aligned} V(x) &= \frac{1}{\sqrt{L}} \sum_{n=-\infty}^{\infty} V_{q_n} e^{iq_n x} \qquad \text{(D.13)} \\ &= \frac{1}{\sqrt{L}} \sum_{n=0}^{\infty} (V_{q_n} e^{iq_n x} + V_{-q_n} e^{-iq_n x}) \\ &= \frac{1}{\sqrt{L}} \sum_{n>0} (|V_{q_n}| e^{iq_n x + i\phi_{q_n}} + |V_{-q_n}| e^{-iq_n x + i\phi_{-q_n}}) \\ &= \frac{1}{\sqrt{L}} \sum_{n>0} |V_{q_n}| (e^{i(q_n x + \phi_{q_n})} + e^{-i(q_n x + \phi_{q_n})}) \\ &= \frac{2}{\sqrt{L}} \sum_{n>0} |V_{q_n}| \cos(q_n x + \phi_{q_n}), \end{aligned}$$

where it has also been used that $V_{q=0} = 0$.

Appendix E

Reduced units

In the simulations the physical constants a, t_1, $\hbar$, and e are set equal to one in order to reduce round-off errors. The table below shows the relation between the reduced units used in the simulations and its SI counterparts. Typical experimental values of the lattice parameter and the tunneling amplitude are $a \sim 1$ Å and $t_1 \sim 1$ eV. An electric field strength of $E^* = 0.01$ in the units used in the simulations corresponds to a field strength of $E = 10^8$ V/m in the SI. In case of a uniform electrostatic field, and a crystal sample of size $r \sim 1$ μm, this would require a potential difference of $U = 10^2$ V.

Quantity	Reduced unit	Relation to SI
Length	r^*	ra^{-1}
Energy	ϵ^*	ϵt_1^{-1}
Action	S^*	$S\hbar^{-1}$
Charge	q^*	qe^{-1}
Electric field strength	E^*	$Eaet_1^{-1}$

Table E.1: Reduced units.

Bibliography

[1] H.B. Nielsen and M. Ninomiya, *The Adler-Bell-Jackiw anomaly and Weyl fermions in a crystal*, Physics Letters B **130**, 389 (1983).

[2] R. Bertlmann, *Anomalies in Quantum Field Theory* (Oxford Universty Press, 2000).

[3] R. Jackiw, *Axial anomaly*, International Journal of Modern Physics A **24**, 659 (2010).

[4] A. Zee, *Quantum Field Theory in a Nutshell* (Princeton Universty Press, 2010).

[5] M. E. Peskin and D. V. Schroeder, *An Introduction to Quantum Field Theory* (Perseus Books Publishing, 1995).

[6] S. L. Adler, *Axial-Vector Vertex in Spinor Electrodynamics*, Physical Review **177**, 2426 (1969).

[7] T. Ohlsson, *Relativistic Quantum Physics: From Advanced Quantum Mechanics to Introductory Quantum Field Theory* (Camebridge Universty Press, 2011).

[8] M. D. Schwartz, *Quantum Field Theory and the Standard Model* (Camebridge Universty Press, 2014).

[9] J. Behrends, A.G. Grushin, T. Ojanen, and J.H. Bardarson, *Visualizing the chiral anomaly in Dirac and Weyl semimetals with photoemission spectroscopy* , Physical Review B **93**, 075114 (2016).

[10] J. S. Bell and R. Jackiw, *A PCAC Puzzle:* $\pi^0 \to \gamma\gamma$ *in the* σ*-Model*, Il Nuovo Cimento A **60**, 47 (1969).

[11] S. M. Girvin and K. Yang, *Modern Condensed Matter Physics* (Cambridge Universty Press, 2019).

[12] M. A. Omar, *Elementary Solid State Physics: Principles and Applications* (Addison-Wesley Pub. Co., 1993).

[13] C. Kittel, *Introduction to Solid State Physics* (John Wiley & Sons, 2005).

[14] N. Ashcroft and N. D. Mermin, *Solid State Physics* (Saunders College Publishing, 1976).

[15] K. Leo, P. Haring Bolivar, F. Brüggemann, R. Schwedler, and K. Köhler, *Observation of Bloch oscillations in a semiconductor superlattice*, Solid State Communications **84**, 943 (1992).

[16] T. Dekorsy, R. Ott, H. Kurz, and K. Köhler, *Bloch oscillations at room temperature*, Physical Review B **51**, 17275 (1995).

[17] B. Yan and C. Felser, *Topological Materials: Weyl Semimetals*, Annual Review of Condensed Matter Physics **8**, 337 (2017).

[18] J. D. Hannukainen, Y. Ferreiros, A. Cortijo, and J. H. Bardarson, *Axial anomaly generation by domain wall motion in Weyl semimetals*, Physical Review B **102**, 241401 (2020).

[19] O. Vafek and A. Vishwanath, *Dirac Fermions in Solids: From High-T_c Cuprates and Graphene to Topological Insulators and Weyl Semimetals*, Annual Review of Condensed Matter Physics **5**, 83 (2014).

[20] H. Fukuyama, R. A. Bari, and H. C. Fogdeby, *Tightly Bound Electrons in a Uniform Electric Field* , Physical Review B **8**, 5579 (1973).

[21] L. E. Ballentine, *Quantum Mechanics: A Modern Development*, 2nd edn, (World Scientific Publishing, 2015).

[22] J.H. Davies, *The Physics of Low-Dimensional Semiconductors: An Introduction.* (Camebridge University Press, 2006).

[23] H.B. Nielsen and M. Ninomiya, *A no-go theorem for regularizing chiral fermions*, Physics Letters B **105**, 219 (1981).

[24] J. Behrends and J. H. Bardarson, *Strongly angle-dependent magnetoresistance in Weyl semimetals with long-range disorder*, Physical Review B **96**, 060201(R) (2017).

[25] R. Shankar, *Principles of Quantum Mechanics* (Springer, 2014).

[26] N. Zettili, *Quantum Mechanics: Concepts and Applications.* (John Wiley & Sons, 2009).

[27] L. Råde and B. Westergren, *Mathematics Handbook for Science and Engineering* (Studentlitteratur, 2004).